UNIVERSITY OF CALIFORNIA SAN DIEGO

Discovery of Natural Products from Tropical Filamentous Marine Cyanobacteria and their Cryopreservation

A Thesis submitted in partial satisfaction of the requirements
for the degree Master of Science

in

Biology

by

Thuan-Ethan Tan Ngo

Committee in charge:

Dr. William Gerwick, Chair
Dr. Eric Allen, Co-Chair
Dr. James Golden
Dr. Lena Gerwick

2023

The Thesis of Thuan-Ethan Tan Ngo is approved, and it is acceptable in quality and form for publication on microfilm and electronically.

University of California San Diego

2023

DEDICATION

This thesis is dedicated to my beloved parents, Vicki Van Nguyen, and Hai Ngo, and to my amazing siblings, Katherine Han Ngo, Emily Han Ngo, Marc An Ngo, Matthieu Loc Ngo, and Timothy Thien Ngo, for their undying support throughout my academic journey.

TABLE OF CONTENTS

LIST OF FIGURES

LIST OF TABLES

LIST OF ABBREVIATIONS

A	Adenylation
ACN	Acetonitrile
BGC	Biosynthetic gene cluster
C	Condensation
CAL	Coenzyme-A ligase
CPA	Cryoprotective agent
DMSO	Dimethylsulfoxide
KR	Ketoreductase
LCMS	Liquid Chromatography with Tandem Mass Spectrometry
MeOH	Methanol
MNP	Marine Natural Product
MT	Methyltransferase
nMT	Nitrogen methyltransferase
NP	Natural Product
NRP	Non-ribosomal peptide
NRPS	Non-ribosomal peptide synthetase
oMT	Oxygen methyltransferase
PCP	Peptidyl carrier protein

ACKNOWLEDGEMENTS

The work in this thesis would not have been possible without support of many people. I would like to first acknowledge Professor William H. Gerwick and Dr. Lena Gerwick for their support as my PIs, mentors, and chairs on my committee. Without their mentorship and support, I would not have been able to become the scientist that I am today. Words cannot express my gratitude for having such supportive and inspirational mentors in this laboratory.

I would also like to acknowledge my other committee members, Professor Eric Allen and Professor James Golden for their time and guidance toward the completion of my projects.

I would like to thank the entire Gerwick lab for their help and support during my program. Special thanks to Andrew Ecker for their wonderful friendship and mentorship in the lab when I was starting out conducting research. My love for research and discovery would not be the same without them. I'd also like to thank Dr. Evgenia Glukhov and Dr. Nicole Avalon for guiding me through my research journey with tutorials on various instruments and valuable feedback on experimental design.

I am also thankful for all the wonderful friends that I've made at UCSD. Without my community and my chosen family, my experience here would have been completely different. Shoutout to my Cuzco, Erlanger, and oSTEM community!

Chapter 2, in full, is currently being prepared for publication. Ngo, Thuan-Ethan; Guild, Rory; Ecker, Andrew; Naman, Ben; Alexander, Kelsey; Gerwick, Lena; Gerwick, William. "Induced production and Biosynthesis of Novel Linear Depsipeptide Hectoramide B, from Marine Cyanobacterium Moorena producens JHB in Competing Co-culture". The thesis author was the primary investigator and author of this paper.

I'd also like to recognize Dr. Ruta Sahasrabudhe who assisted in the sequencing that was carried out by the DNA Technologies and Expression Analysis Core at the UC Davis Genome Center, supported by NIH Shared Instrumentation Grant 1S10OD010786-01. I'd also like thank Dr. Vikram Shende and Andrew Ecker on their assistance with the generation of structural data of hcaB adenylation domain.

Chapter 3, in part, has been facilitated by the work of Syrena Whitner, Nathan Moss, Andrew Ecker, Sebastian Rohrer, and Yifan He. Their previous work on developing a cryopreservation method for the cyanobacteria have paved the way for these optimization studies. I'd also like to acknowledge Dr. Evgenia Glukhov for providing the cultures used in this work and for feedback on growth recovery and health of the cultures.

Lastly, I am extremely thankful to all of my family members and my dog Fitz who's love, and support have carried me through my program and academic journey.

ABSTRACT OF THE THESIS

Discovery of Natural Products from Tropical Filamentous Marine Cyanobacteria and their Cryopreservation

by

Thuan-Ethan Tan Ngo

Master of Science in Biology

University of California San Diego, 2023

Dr. William Gerwick, Chair
Dr. Eric Allen, Co-Chair

Marine cyanobacteria are a rich source of biologically relevant molecules with diverse therapeutic bioactivity and structural diversity. Many natural products have been isolated and characterized from marine cyanobacteria, however, bioinformatic analyses into their genomes have revealed the wealth of biosynthetic gene clusters yet to be linked to any known natural products. In this work, we sought to further explore the metabolic potential of these cyanobacteria and work toward conservation of these precious biological resources. We discovered a novel linear depsipeptide, hectoramide B, from the tropical filamentous cyanobacteria, *Moorena producens* JHB, through a co-culture competition experiment. We further identified the putative biosynthetic gene cluster associated with hectoramide B.

Additionally, we successfully developed and optimized cryopreservation methods for some of the cyanobacterial strains within the Gerwick lab collection. In conclusion, alternative methods, like co-culture competition experiments, can be employed to discover novel compounds from this rich source of natural products. Additionally, cryopreservation can be a valuable tool for the long-term preservation of these cultures. Both avenues can further develop the field of marine natural products toward novel drug discovery and conservation efforts of these valuable biological resources.

Chapter 1: General Introduction

1.1 Brief introduction to the field of natural products

Long before humans extracted and isolated natural products for medicinal purposes from living organisms, Nature has selected for – through evolutionary pressures – the production of specialized secondary metabolites. Secondary metabolites, or natural products, differ from other molecules produced by primary metabolism, such as energy or anabolic pathways, because they are non-essential but provide organisms from all kingdoms of life benefits in communication, defense, and attack. Humans have learned to leverage these natural resources even before the advent of modern technology. For instance, one of the earliest records of human applications of naturally derived compounds was documented in Mesopotamia in 2600 B.C. where oils extracted from plants such as *Cedrus* species (cedar) and *Papayer somniferum* (poppy juice) were used to treat maladies like coughs, colds, and inflammation (Cragg & Newman, 2005). Thousands of years later, some of these extracts are still being used in traditional medicine or have inspired the development of modern drugs by improving the efficacy of the original natural product through medicinal chemistry.

Many of the first natural products to be isolated and characterized have terrestrial origins. Some examples that are still being used today include morphine **(1)** (used as an analgesic), acetylsalicylic acid **(2)** (anti-inflammatory), and penicillin **(3)** (antibiotic) (Figure 1.1). Morphine was isolated from *P. somniferum* by Friedrich Serturner in 1816 and later became the first commercially available natural product for therapeutic use in 1826 by Merck™ (Cragg & Newman, 2005). Acetylsalicylic acid, or more commonly known as aspirin, was extracted from the bark of the willow tree (*Salix alba L.*), and was later commercialized by Bayer™ in 1899.

Lastly, penicillin, which is derived from the fungus, *Penicillium notatum*, was isolated by Alexander Fleming in 1929 and has completely revolutionized the field of drug discovery and antibiotic development. Over the last four decades, nearly 2000 drugs derived from or inspired by natural products have been FDA approved for clinical use for a variety of therapeutic application (Newman & Cragg, 2020). Evidently, natural products derived from terrestrial sources have provided humans with diverse bioactivity and has greatly changed the state of medicine and human health. With such rich diversity found on land, it is only natural that we turn to the sea in search of new compounds.

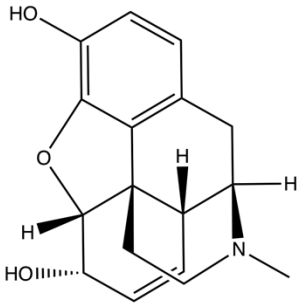

Morphine (1)

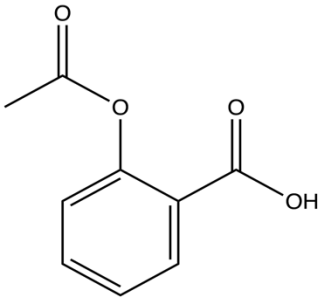

Acetylsalicylic acid (2)

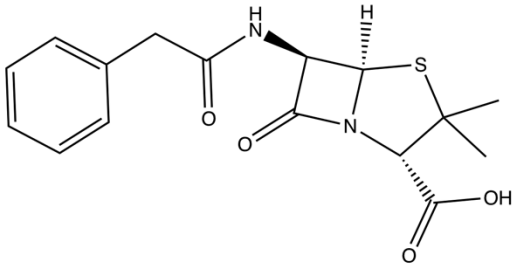

Penicillin (3)

Figure 1.1 Structures of some of the first terrestrial natural products to be FDA approved for clinical use

1.2. Marine natural products

Despite over 100 years of research in terrestrial natural products, the field of marine natural products is still relatively new. One of the main barriers to the early expansion of this field of research was largely the inaccessibility of regions beyond the intertidal or near-shore. Subsequently, many of the first marine species to be investigated for natural product production were those that could be easily identified and collected near-shore such as red algae, sponges, and soft corals (Gerwick & Moore, 2012). For example, one of the earliest findings that had clinical application was an anticancer drug and synthetic nucleoside analogue cytarabine **(4)** from a Caribbean sponge, *Cryptotheca crypta*, which later became the first FDA approved marine anticancer agent in 1969 (Montaser & Luesch, 2011; Schwartsmann et al., 2001). Although our oceans cover 70% of earth's surface and is home to millions of marine species, much of this biodiversity has been left unexplored due to technological limitations. However, due to recent developments in natural products discovery pipeline such as sampling techniques, extraction protocols and biotechnology, we have been able to investigate deeper depths of the ocean and more specifically the world of marine microorganisms. For instance, researchers from the Fenical and Jensen group at the Scripps Institution of Oceanography developed a deep-sea sediment collection apparatus that allowed them to discover new marine actinomycetes strains that have great potential for novel secondary metabolite production (Fenical & Jensen, 2006). Furthermore, improved, and automated extraction protocols combined with bioassay guided fractionation has allowed for high throughput screening of biological material for novel secondary metabolites in resource-limited settings (Gerwick & Moore, 2012). Lastly, developments in biotechnology, fermentation, and DNA sequencing methods have made it possible to identify new biosynthetic gene clusters through genome mining and subsequently,

new natural products without the need for substantial quantities of biological material (Montaser & Luesch, 2011). These developments have led to a new era of marine natural products and drug discovery. It has greatly allowed researchers to discover novel chemical scaffolds and compounds displaying interactions with diverse drug targets.

At the time that this is being written, there are only a handful of drugs derived from marine sources that have been approved for clinical use and more that are undergoing Phase I-III clinical trials due to the novelty of the field (Ghareeb et al., 2020; Newman & Cragg, 2016). As an example, Brentuximab Vedotin 63 (Adcetris®) became FDA approved in 2011 for the treatment of Hodgkin lymphoma and systemic anaplastic large cell lymphoma and was derived from Dolastatin 10 **(5)** which was collected from an Indian Ocean Sea hare, *Dolabella Auricularia* (Ghareeb et al., 2020; Pettit et al., 1987). Another example is Ziconotide **(6)** (Prialt®) which is an analogue of ω-conotoxin from the sea snail, *Conus magus* **(Figure 1.2)**. It gained FDA approval in 2004 as an analgesic agent and functions as an N-type voltage-gated calcium channel blocker (Ghareeb et al., 2020; McGivern, 2007; McIntosh et al., 1982). Undoubtedly, natural products derived from marine sources have the potential for diverse clinical applications and are important for drug discovery efforts due to the diverse chemical scaffolds and novel bioactivity.

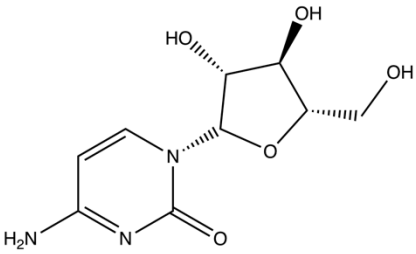

Cytarabine (4)

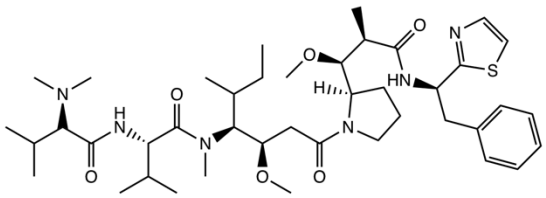

Dolastatin 10 (5)

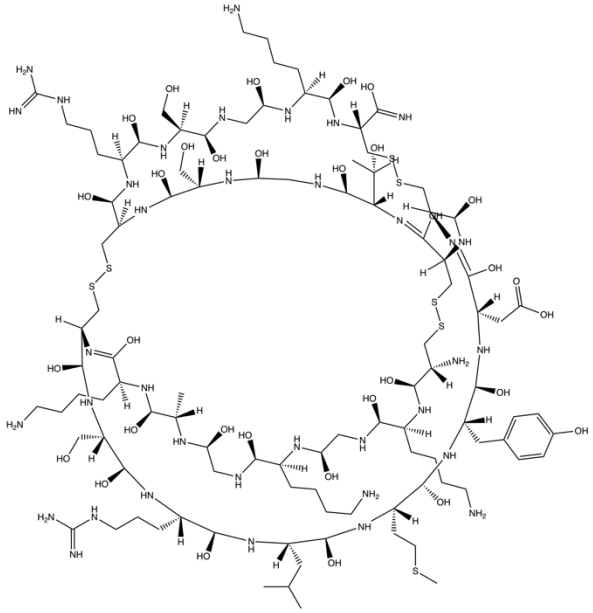

Ziconitide (6)

Figure 1.2 Structures of natural products derived from marine sources that are currently FDA approved for clinical use.

1.3 Marine Cyanobacteria natural products

Cyanobacteria are a rich source of bioactive relevant molecules. In a review of natural products derived from cyanobacteria conducted by Demay *et al.*, 1630 unique molecules were identified from different publications and grouped into 260 families of metabolites that had varying bioactivities such as cytotoxicity, anti-inflammatory, and antimicrobial activity (Demay et al., 2019). Furthermore, genome mining efforts have revealed that there is a wealth of biosynthetic pathway diversity in gene clusters related to secondary metabolism, a majority of

which are not associated to a known product and belong to unique gene cluster families (Calteau et al., 2014; Dittmann *et* al., 2015). Clearly, cyanobacteria have great potential in secondary metabolite production with attractive bioactivity for drug discovery efforts. However, there is still much to explore considering that of the 39,238 compounds currently listed on the MarinLit database, a repository of the latest publications and compounds related to marine natural products, only 965 compounds have been identified in marine cyanobacteria. Therefore, there is now a great effort put on researchers to develop a multidisciplinary approach to natural product discovery. Creative and more precise strategies in genomics, proteomics, and metabolomics, such as molecular networking and genome mining, will contribute to the ongoing discovery of natural products in marine cyanobacteria.

As mentioned above, creative, and more precise genomics, metabolomics, and proteomics, will contribute to the continued discovery of novel chemical and biosynthetic diversity in marine cyanobacteria. Moreover, these efforts will aid in advancements in biotechnology, synthetic biology, medicinal chemistry, and subsequently drug discovery pipelines.

1.4 General Thesis Contents

Chapter 2 details my efforts to identify the biosynthetic gene cluster that is responsible for the production of a novel secondary metabolite, hectoramide B, from the marine cyanobacterium, *Moorena producens* JHB and characterize its bioactivity. The scope of this work includes regeneration of sequencing data and assembly of the *M. producens* JHB genome, bioinformatic analyses to identify the putative biosynthetic gene cluster, re-isolation of pure compound and antifungal susceptibility testing against *Candida albicans*.

Chapter 3 summarizes the attempts at developing a cryopreservation method that is suitable for the cyanobacteria species that are maintained in the Gerwick lab. These cyanobacterial cultures include species from the genera *Moorena, Leptolyngbya, Okeania,* and *Spirulina*. Varying factors including freezing rate, thaw rate, and cryoprotective agent selection were tested to develop the most optimal method for growth recovery and long-term storage.

References

Calteau, A., Fewer, D. P., Latifi, A., Coursin, T., Laurent, T., Jokela, J., Kerfeld, C. A., Sivonen, K., Piel, J., & Gugger, M. (2014). Phylum-wide comparative genomics unravel the diversity of secondary metabolism in Cyanobacteria. *BMC Genomics*, *15*(1), 977. https://doi.org/10.1186/1471-2164-15-977

Cragg, G. M., & Newman, D. J. (2005). Biodiversity: A continuing source of novel drug leads. *Pure and Applied Chemistry*, *77*(1), 7–24. https://doi.org/10.1351/pac200577010007

Demay, J., Bernard, C., Reinhardt, A., & Marie, B. (2019). Natural Products from Cyanobacteria: Focus on Beneficial Activities. *Marine Drugs*, *17*(6), 320. https://doi.org/10.3390/md17060320

Dittmann, E., Gugger, M., Sivonen, K., & Fewer, D. P. (2015). Natural Product Biosynthetic Diversity and Comparative Genomics of the Cyanobacteria. *Trends in Microbiology*, *23*(10), 642–652. https://doi.org/10.1016/j.tim.2015.07.008

Fenical, W., & Jensen, P. R. (2006). Developing a new resource for drug discovery: Marine actinomycete bacteria. *Nature Chemical Biology*, *2*(12), 666–673. https://doi.org/10.1038/nchembio841

Gerwick, W. H., & Moore, B. S. (2012). Lessons from the past and charting the future of marine natural products drug discovery and chemical biology. *Chemistry & Biology*, *19*(1), 85–98. https://doi.org/10.1016/j.chembiol.2011.12.014

Ghareeb, M. A., Tammam, M. A., El-Demerdash, A., & Atanasov, A. G. (2020). Insights about clinically approved and Preclinically investigated marine natural products. *Current Research in Biotechnology*, *2*, 88–102. https://doi.org/10.1016/j.crbiot.2020.09.001

McGivern, J. G. (2007). Ziconotide: A review of its pharmacology and use in the treatment of pain. *Neuropsychiatric Disease and Treatment*, *3*(1), 69–85. https://doi.org/10.2147/nedt.2007.3.1.69

McIntosh, M., Cruz, L. J., Hunkapiller, M. W., Gray, W. R., & Olivera, B. M. (1982). Isolation and structure of a peptide toxin from the marine snail Conus magus. *Archives of Biochemistry and Biophysics*, *218*(1), 329–334. https://doi.org/10.1016/0003-9861(82)90351-4

Montaser, R., & Luesch, H. (2011). Marine natural products: A new wave of drugs? *Future Medicinal Chemistry*, *3*(12), 1475–1489. https://doi.org/10.4155/fmc.11.118

Newman, D. J., & Cragg, G. M. (2016). Drugs and Drug Candidates from Marine Sources: An Assessment of the Current "State of Play." *Planta Medica*, *82*(9/10), 775–789. https://doi.org/10.1055/s-0042-101353

Newman, D. J., & Cragg, G. M. (2020). Natural Products as Sources of New Drugs over the Nearly Four Decades from 01/1981 to 09/2019. *Journal of Natural Products*, *83*(3), 770–803. https://doi.org/10.1021/acs.jnatprod.9b01285

Pettit, G. R., Kamano, Y., Herald, C. L., Tuinman, A. A., Boettner, F. E., Kizu, H., Schmidt, J. M., Baczynskyj, L., Tomer, K. B., & Bontems, R. J. (1987). The isolation and structure of a remarkable marine animal antineoplastic constituent: Dolastatin 10. *Journal of the American Chemical Society*, *109*(22), 6883–6885. https://doi.org/10.1021/ja00256a070

Schwartsmann, G., da Rocha, A. B., Berlinck, R. G., & Jimeno, J. (2001). Marine organisms as a source of new anticancer agents. *The Lancet Oncology*, *2*(4), 221–225. https://doi.org/10.1016/S1470-2045(00)00292-8

Chapter 2: Induced production and Biosynthesis of Novel Linear Depsipeptide Hectoramide B from Marine Cyanobacterium *Moorena producens* JHB in Competing Co-culture

2.1 Abstract

The tropical marine cyanobacterium *Moorena producens* JHB (JHB) is a valuable source of secondary metabolites with therapeutically applicable bioactivity. Investigations into the metabolic profile of this strain have led to the discovery of a few novel compounds such as hectochlorin and jamaicamide, but bioinformatic analyses of the genome of JHB have suggested that there are many more cryptic gene clusters to be unlocked. In order to stimulate the production of novel compounds from JHB, we performed a co-culture competition experiment with *Candida albicans* to simulate a microbial antagonistic relationship. We observed the possible upregulation of a new compound, hectoramide B. Through bioinformatic analysis of the reassembled genome of JHB, we were able to identify the putative biosynthetic gene cluster responsible for the production of hectoramide B. In conclusion, co-culture competition experiments are a valuable method to facilitate the discovery of novel natural products from cyanobacteria. Further studies will need to be conducted to confirm the identity of this BGC as well as investigations into what other cryptic gene clusters we can unlock from this strain.

2.2 Introduction

Cyanobacteria from the genus *Moorena* are a prolific source of bioactive secondary metabolites. Representatives of this genus are tropical, filamentous, photosynthetic, and non-diazotrophic cyanobacteria that reside in the marine benthic zone (Engene *et al*., 2012). Many diverse secondary metabolites, or natural products (NP), have been isolated from various species of this genus. As an example, curacin A, a novel lipid with thiazoline-containing structure, was

isolated in 1994 from *Moorena producens* 3L and was found to have antimitotic, antiproliferative, and brine shrimp toxicity bioactivity via inhibition of microtubule assembly (Gerwick *et al*., 1994, p. 199). Another interesting example is the cyclic depsipeptide apratoxin A which was isolated in 2001 from *Moorena bouillonii* PNG (Luesch *et al*., 2001). Apratoxin A was found to exhibit potent cytotoxicity via binding and targeting Sec61a, the central subunit of the protein translocation channel which subsequently blocks protein translocation (Liu *et al*., 2009; Paatero *et al*., 2016). Comparative genomics of species in the *Moorena* genus have revealed the extensive biosynthetic potential of these marine cyanobacteria. The average number of biosynthetic gene clusters (BGCs) present in this genus is generally much higher than other cyanobacteria with ~18% of their genomes dedicated to secondary metabolism (Leao *et al*., 2017). Furthermore, there are a fair number of silent, or cryptic, gene clusters that have still yet to be explored. The genomic potential of these cyanobacteria does not completely align with the metabolic potential because many of these cryptic secondary metabolites may be produced in minor quantities. Without sufficient production of those cryptic natural products, it is difficult to conduct biological activity assays or structure elucidation. Therefore, different methods need to be further explored in order to induce the production of these NPs.

Co-culture experiments are a tried-and-true method for inducing the production of cryptic NPs produced by 'silent' biosynthetic gene clusters. In the ocean, microbes, such as bacteria, viruses, and fungi, are often competing with one another for resources and nutrients. To aid in defense and offense against other microbes, their genomes may encode for production of adaptive secondary metabolites. On the other hand, microbial cultures in a laboratory setting are often grown as axenic monocultures, meaning without other living organisms than the species of interest. Subsequently, their metabolite production may not be accurately representative of their

metabolic potential. Therefore, culturing two organisms together in a laboratory setting can simulate an antagonistic interaction that can induce the production of novel, bioactive secondary metabolites. For example, when Oh and others (2007) co-cultured the marine-derived fungus, *Emericella* sp., and marine actinomycete, *Salinispora arenicola*, together, they discovered a 100-fold increase of two novel antimicrobial compounds produced by *Emericella* sp., emericellamides A and B (Oh *et al*., 2007). In this way, we can partially simulate the natural, ocean environment in order to unlock metabolic pathways that would otherwise, remain silent. Conducting co-culture experiments could be a promising way to discover various new secondary metabolites from marine cyanobacteria.

The tropical filamentous marine cyanobacterium *Moorena producens* JHB (hereto after referred to as JHB) is an excellent producer of bioactive secondary metabolites. JHB was collected on August 22, 1996 at Hector Bay, Jamaica from a shallow depth of 2 meters and has been maintained with saltwater-BG11 (SWBG11) media since its original collection (Marquez *et al.,* 2002). It has been found to produce several useful NPs: hectoramide, hectochlorin A-D, and jamaicamide A-F (Boudreau *et al*., 2015; Edwards *et al*., 2004; Marquez *et al*., 2002). Hectochlorin has been found to have antifungal properties and induces actin polymerization which results in some levels of cytotoxicity. Jamaicamide A-C have sodium channel blocking activity and toxicity to fish. Although this strain's metabolite profile has been extensively studied, genome analysis has revealed that there are as many as 42 cryptic gene clusters yet to be investigated – 11 of which are nonribosomal peptide synthetase (NRPS)-related genes (Leao *et al*., 2017). Therefore, with the correct stimulation, there are many more NPs that could be discovered from this strain of marine cyanobacteria.

The opportunistic pathogenic yeast, *Candida albicans* (*C. albicans)*, is an excellent model for co-culture experiments because its resistance mechanisms against antifungal drugs are well studied and it can lead to the production of a promising bioactive, antifungal natural product (Kabir et al., 2012). *C. albicans* is a yeast that exists in the gastrointestinal and genitourinary tracts of most humans. However, overproduction of this yeast can lead to candida-related illnesses like thrush, vaginal candidiasis, and invasive candidiasis. This is especially harmful to immunocompromised patients such as HIV-infected individuals, transplant recipients, and chemotherapy patients (Kabir *et al*., 2012). Globally, *C. albicans* is the leading cause of candida-related illnesses and without treatment, can result in mortality in 15-35% of adults and 10-15% in neonates (Guinea, 2014). Additionally, infection with *Candida* typically results in extended length of stays for patients in hospitals, higher associated medical costs, and increased mortality (Lockhart, 2014). Luckily, there are antifungal drugs that are regularly used for treatment such as fluconazole, voriconazole, and caspofungin. However, with growing antifungal resistance, particularly in non-albicans strains, there is a great need to reinforce our arsenal of antifungal drugs.

We therefore selected JHB and *C. albicans* for a co-culture experiment in order to potentially identify novel compounds from JHB. We hypothesized that co-culturing these two organisms would form an antagonistic relationship that would potentially lead to the production of a novel compound with antifungal biological activity. In relation to the novel compound that was in fact discovered through such a co-culture experiment, our goals were to (1) re-isolate and characterize the novel compound, (2) elucidate its structure, (3) identify the biosynthetic gene cluster responsible for its production, and (4) characterize its bioactivity, specifically its antifungal properties.

2.3 Results and Discussion

2.3.1 Co-culture experiments with *C. albicans* and *M. producens JHB*

The marine cyanobacterium *M. producens* JHB and fungal pathogen *C. albicans* were co-cultured for 30 days at 27°C with the goal of establishing an antagonistic relationship that would facilitate the discovery of novel natural products from JHB. At the end of the fermentation, there was clear growth of *C. albicans* and JHB had no clear changes in its morphology or color. Crude extracts from the co- and mono-cultures were obtained and screened by liquid chromatography with tandem mass spectrometry (LCMS) to obtain metabolic profiles. A distinct major peak (**Figure 2.1)** in the co-culture was identified to have molecular weight 626.80 ($[M + H]^+$ *m/z* at 627.12, $[M + Na]^+$ *m/z* at 649.30). Other previously characterized compounds were also identified in the crude extract such as, hectochlorin (665.6 *m/z*), jamaicamide A (56 *m/z*) and jamaicamide C (491.1 *m/z*). To calculate the relative abundance of these metabolites in the co- and mono-cultures, the base peak height of hectoramide B, jamaicamide A and jamaicamide C were compared to the base peak height of hectochlorin. There was a significant upregulation of hectoramide B in the co-culture compared to the mono-culture (**Fig. 2.2**). Notably, jamaicamide A and C were also found to be upregulated in the co-culture, but it was not statistically significant. Since this novel peak was found to be potentially upregulated in a co-culture experiment, it was possible that it had some level of antifungal bioactivity. As a result, this compound was isolated to elucidate its molecular structure.

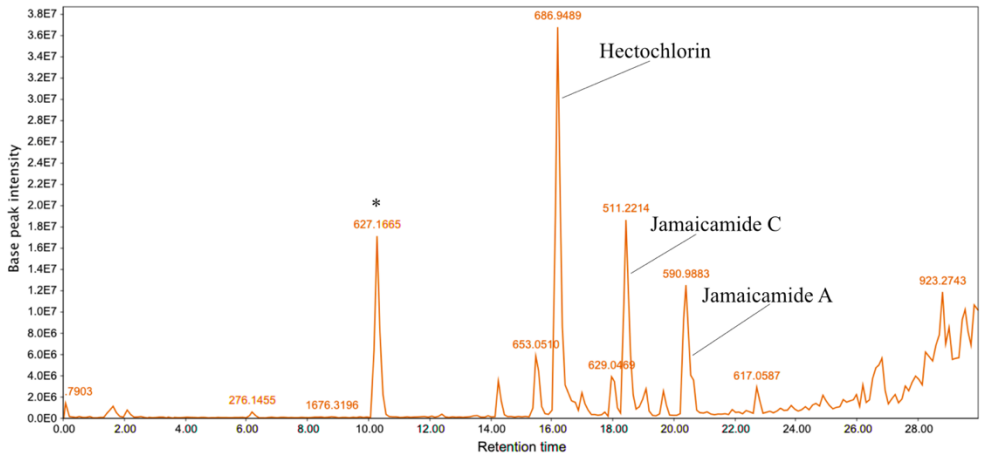

Figure 2.1 Metabolic profile of co-culture crude extract reveals novel distinct peak of 627 *m/z* Chromatogram of co-culture crude extract contains a few previously described metabolites: hectochlorin, jamaicamide C, and jamaicamide A. Novel peak is indicated by asterisk (*).

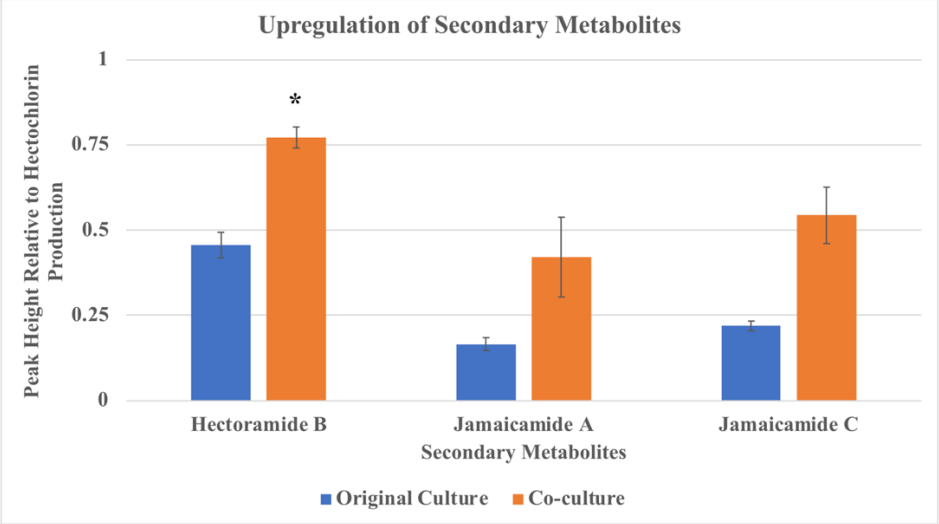

Figure 2.2 Bar graph of upregulation of secondary metabolites from co-culture of M. producens JHB and C. albicans. Relative production of secondary metabolites produced by M. producens JHB identified by LCMS. Base peak height of hectoramide B, jamaicamide A, and jamaicamide C was compared to base peak height of hectochlorin production. The standard error bars for each mean are presented. *P < 0.01

2.3.2 Isolation and Structure Elucidation of Hectoramide B

Initial structure elucidation efforts focused on the LC-MS/MS networking of metabolites and subsequent clustering based on fragmentation pattern of a metabolite with *m/z* of 627.12. A node was identified that connected 627.12 *m/z* to the previously characterized hectoramide A (**Figure 2.2**). This information in combination with ^{1}H, ^{13}C, HSQC, HMBC, and COSY data suggests that this molecule is indeed structurally related to hectoramide A with the emergence of

a new set of NMR peaks corresponding to the addition of an *N,N*-dimethyl-*O*-methyltyrosine. Therefore, hectoramide A is likely a degradation product of hectoramide B, either through an artificial hydrolysis or a possible enzymatic process. Given the structure of hectoramide B, we were now able to investigate which biosynthetic gene cluster was associated with its production.

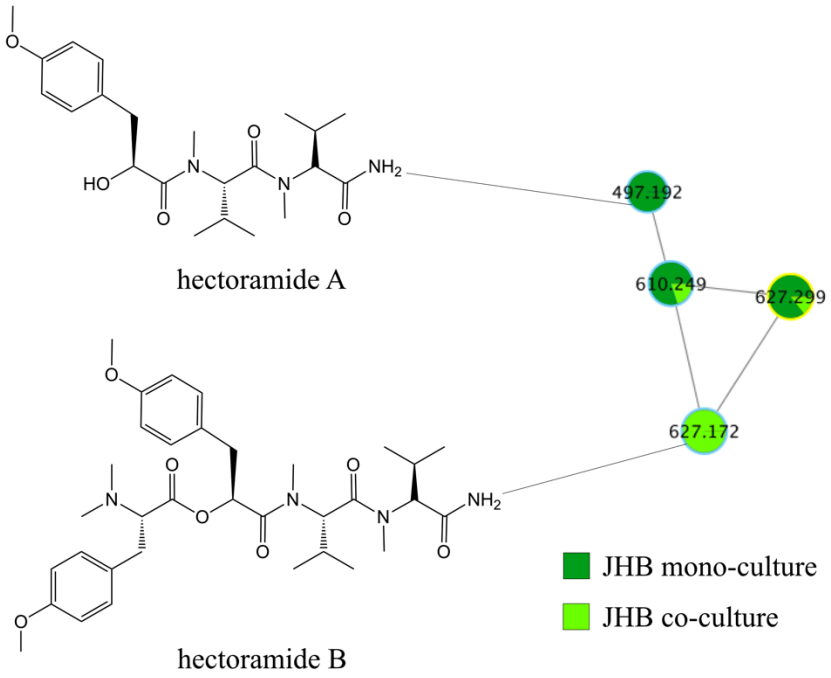

Figure 2.3 The hectoramide B cluster of nodes within the molecular network of *Moorena producens* JHB
The previously characterized hectoramide A (497.19 m/z) is clustered with hectoramide B (627.17 m/z). Dark green nodes are JHB monoculture, light green nodes are JHB+CA co-culture.

2.3.3 Retrobiosynthetic scheme of Hectoramide B

A retrobiosynthetic scheme of the hectoramide B biosynthetic gene cluster was developed based on its chemical structure, including modules consistent with a non-ribosomal peptide synthetase (NRPS) and tailoring enzymes for key functional groups (**Figure 2.4**). Non-ribosomal peptides (NRP) are typically synthesized in a colinear manner where each module encodes for the incorporation of an amino acid residue. Therefore, we are able to predict the architecture of a biosynthetic gene cluster based on the chemical structure of hectoramide B. We

hypothesized that the initial module would be a NRPS that would contain an adenylation (A) domain that encodes for the incorporation of tyrosine followed by methyltransferase domains that would catalyze the methylation of the oxygen on tyrosine and the nitrogen of the amine group of tyrosine. We predict that module 2 would be a depsipeptide synthetase that will incorporate an α-keto acid version of tyrosine that is reduced to 2-hydroxy-3-(4-hydroxyphenyl) propanoic acid by a ketoreductase domain, followed by methylation of the oxygen on tyrosine by an oxygen-methyltransferase domain. Modules 3 and 4 are predicted to contain A domains that will incorporate valine residues followed by methylation by a *N*-methyltransferase. A terminal amidation reaction should be present after module 4, possibly related to one seen in carmabin A and vatiamide A biosynthesis (Balunas et al., 2010; Hooper et al., 1998; Moss et al., 2019). Additionally, after module 4 there is predicted a thioesterase (TE) domain that will assist in termination of the chain and release of hectoramide B.

Preliminary investigation into the *M. producens* JHB genome (GenBank Accesion Number: CP017708 version CP017708.1) revealed a potential candidate BGC for hectoramide B (Leao et. al 2017). However, based on the retrobiosynthetic scheme, this BGC did not contain the third and fourth modules that are responsible for the incorporation of two valine residues and termination of the biosynthesis. Therefore, we sought to generate more sequencing data and reassemble the genome with the goal of improving the quality of the assembly and provide enough coverage to capture the BGC that is responsible for the production of hectoramide B.

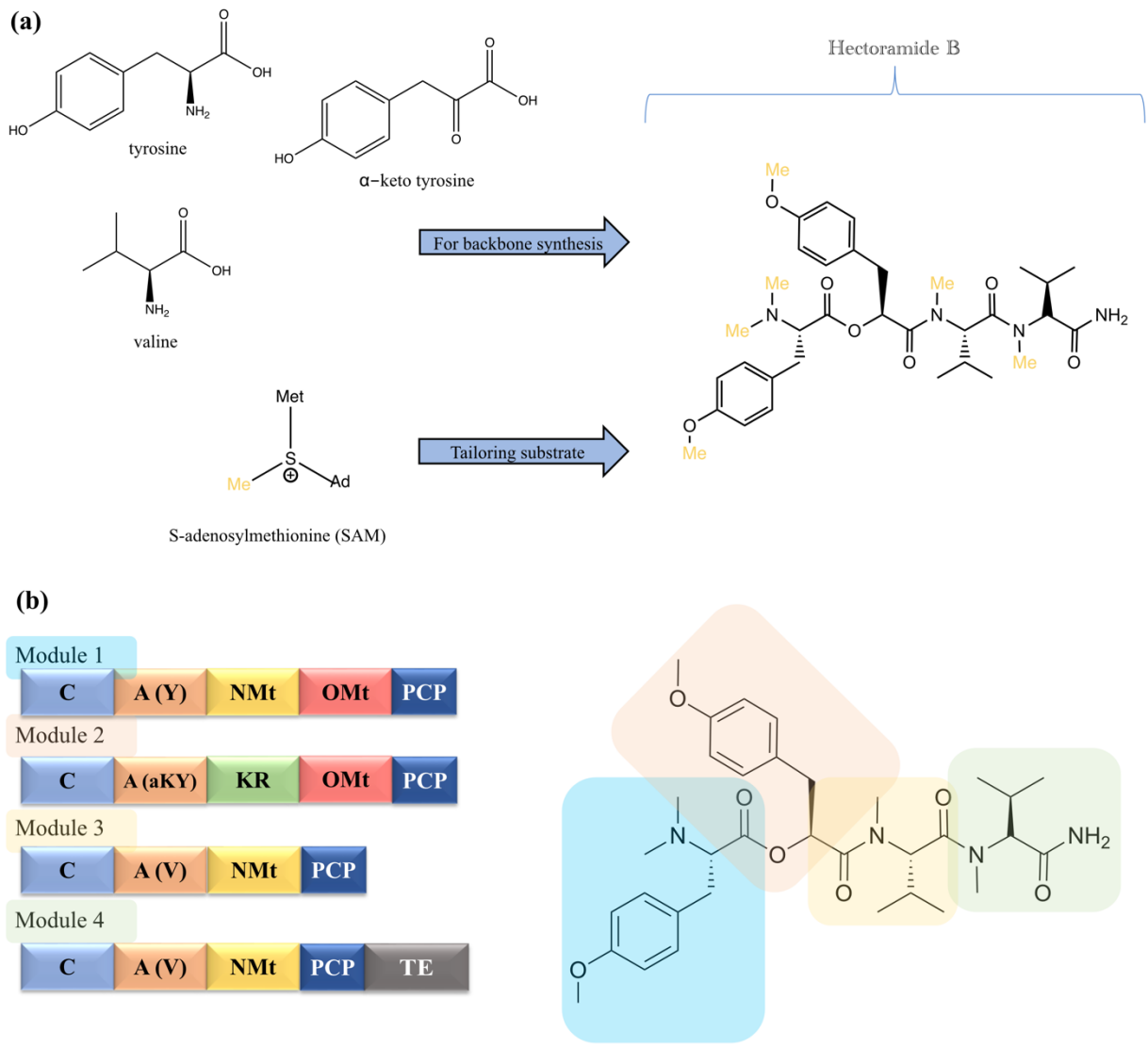

Figure 2.4 Retrobiosynthetic Scheme of Hectoramide B. a) Structure and biosynthetic precursors associated with hectoramide B biosynthesis
Backbone synthesis is proposed to result from incorporation of tyrosine followed by α-keto acid version of tyrosine, and two valine residues. Methylations are proposed to result from SAM-dependent methyltransferase domains. (b) Predicted modular organization of hectoramide B biosynthetic gene cluster. Squares represent enzymatic domains. C: condensation domain, A(Y): adenylation domain for tyrosine, A(akY): adenylation domain for α-keto tyrosine, A(V): adenylation domain for valine, KR: ketoreductase domain, NMt: Nitrogen-methyltransferase domain, OMt: oxygen-methyltransferase domain, PCP: peptidyl-carrier protein.

2.3.4 Improvement of genome assembly of *M. producens* JHB

Data generation and assembly

The *M. producens* JHB DNA was extracted and subjected to nanopore long read sequencing. A subset of the sequencing data was generated using Filtlong. Due to the high

number of short fragments generated from Nanopore sequencing, the parameters were chosen to filter out the reads of poorest quality and length. After the filtering step, 65,047 reads and 1,500,008,648 total read lengths were passed.

The remaining reads were assembled using Flye and Unicycler. After the Flye long-read only assembly, 9 bins were generated by Metabat2 and annotated by CheckM. Similarly, after the Unicycler long-read assembly and hybrid assembly, 8 and 12 bins, respectively, were generated and annotated. Bins that contained assemblies with ~43.67% GC content and contig length of ~9Mbp were selected for genome polishing.

Genome polishing and genome assembly assessment

Table 2.1 shows BUSCO evaluation result for each assembly tool and polishing combination. There are 773 BUSCO genes associated with the cyanobacteria_odb10 dataset that was used for evaluation in this study.

The assembly with the program SPades using Illumina short-reads, that was conducted prior to this study, showed 756 single copies and 8 duplicated genes and the completeness was 98.8%. There were 4 genes missing and 5 were fragmented. Long-read sequencing usually has higher error rates but the assembly of contigs is typically improved as compared with short-read sequencing assemblies (Logsdon et al., 2020). Combining short-reads and long-reads typically results in the best assembly because you get maximum coverage with long-reads and sequence correction with the short-reads. Based on the BUSCO (Manni et al., 2021) evaluation, hybrid assembly with Unicycler and Flye and pilon combination resulted in the best assemblies. Both assembly methods resulted in 99.2% completeness. However, the Flye+pilon assembly resulted in a single contig of 9Mbp. Therefore, we selected this assembly for BGC analysis using AntiSMASH (GenBank Accession Number: CP017708.2).

Table 2.1 Evaluation of the Quality of Genome Assembly Based on Quast and BUSCO

Assembly method	# of contigs	N50	Total length	GC (%)	# Mismatches	# of Complete Single	# of Complete duplicated	Fragmented	missing	Completeness
SPades	3	9373345	9384763	43.7	26015	756	8	5	4	98.84
Unicycler long-read	2	8738093	9632771	43.6	0	460	9	202	102	60.67
Unicycler hybrid	2	5885695	9639251	43.7	0	759	8	2	4	99.22
Flye	1	9645659	9645659	43.6	0	610	5	108	50	79.56
Flye + Pilon	1	9648534	9648534	43.7	0	759	8	2	4	99.22

2.3.5 Putative Biosynthetic Gene Cluster of Hectoramide B

Detailed inspection of the *M. producens* JHB genome revealed one candidate biosynthetic gene cluster that is, putatively, involved in the biosynthesis of hectoramide B and will be referred to as the hectoramide B (*hca)* pathway for brevity. The overall genetic architecture and domain organization encountered in this cluster is consistent with the retrobiosynthetic scheme described above (MiBIG Accession number: BGC0002754) (**Figure 2.4)**. In this analysis, we integrated BGC annotations predicted by AntiSMASH with information from protein family homology analysis, substrate selectivity prediction, and active site and motif identification. This analysis supports the hypothesis that this 41,683 bp BGC is most likely responsible for hectoramide B production (**Figure 2.5, Table 2.2)**. The *hca* pathway is comprised of 4 core biosynthetic NRPS modules that are predicted to operate in a co-linear fashion. The pathway genes are flanked by putative regulatory genes, transport-related genes, and coding regions for hypothetical proteins, providing provisional boundaries to the biosynthetic cluster. Overall, this putative biosynthetic gene cluster also supports NMR spectra data gathered for the structure of hectoramide B.

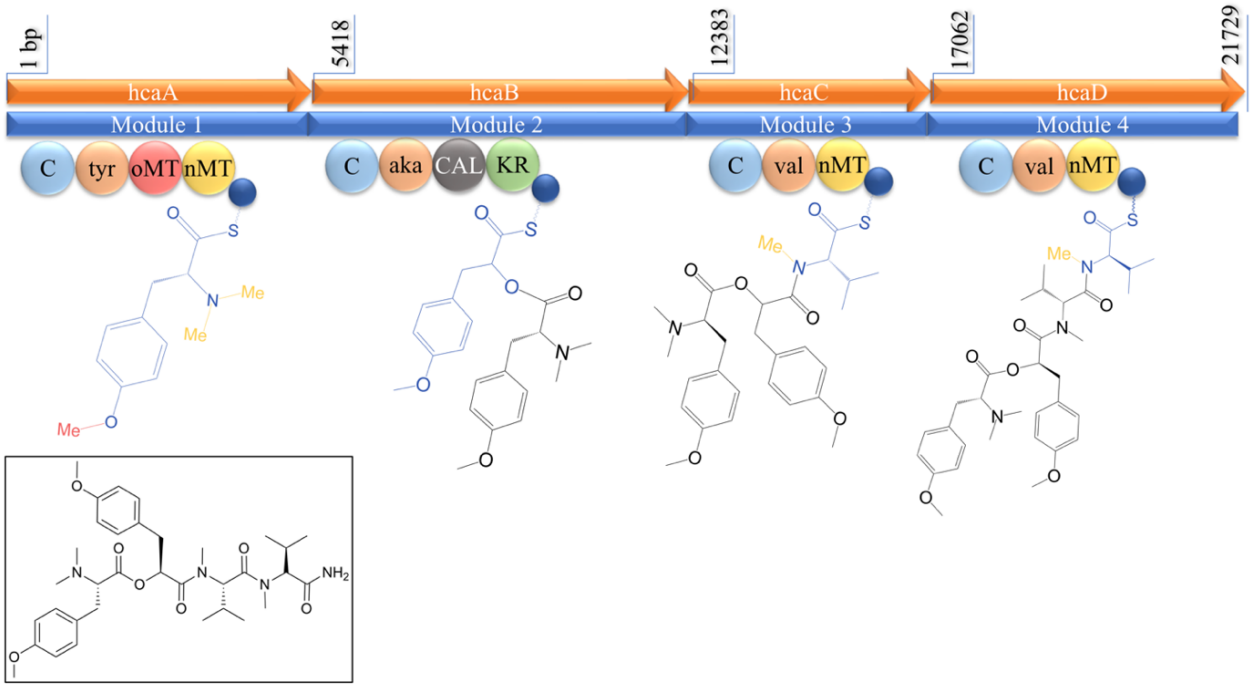

Figure 2.5 Putative biosynthetic gene cluster for hectoramide B
There are 4 core biosynthetic modules organized in a colinear fashion in the *hca* pathway. Transport-related genes, regulatory genes and other hypothetical proteins were not included in this figure. The BGC was generated based on Antismash output, Pfam analysis, sequence alignments, substrate selectivity prediction, and protein modelling. The structure of hectoramide B is presented in the box. C: condensation domain, tyr: adenylation domain for tyrosine incorporation, oMT: oxygen methyltransferase domain, nMT: nitrogen methyl transferase domain, aka: adenylation domain for α–keto acid tyrosine incorporation, CAL: co-enzyme A ligase domain, KR: ketoreductase domain, val: adenylation domain for valine incorporation, small blue circles represent acyl-carrier proteins. Phosphopantathiene arms are symbolized by wavy lines. Orange arrows indicate biosynthetic genes.

Table 2.2 Deduced Functions of the Open Reading Frames in the *hca* Gene Cluster

Protein	**Amino acids**	**Proposed function**
ORF 1	275	PGAP-1 like protein
ORF 2	723	SARP family Transcriptional regulator
ORF 3	72	Beta-keto-acyl synthase
hcaA (Module 1)	1892	Tyrosine
C	60-356	condensation domain
A	534-926	adenylation domain
oMT	1013-1139	*O*-methyltransferase
nMT	1369-1587	*N*-methyltransferase
PCP	1799-1866	Peptidyl-carrier protein
hcaB (Module 2)	2316	4-Hydroxyphenylpyruvate (acid)
C	72-371	condensation domain
A	535-914	adenylation domain
CAL	1127-1543	Coenzyme-A ligase domain
KR	1890-2087	Ketoreductase domain
PCP	2223-2290	Peptidyl-carrier protein
hcaC (Module 3)	1564	Valine
C	73-373	condensation domain
A	543-945	adenylation domain
nMT	1038-1260	*N*-methyltransferase
PCP	1469-1535	Peptidyl-carrier protein
hcaD (Module 4)	1959	Valine
C	75-372	condensation domain
A	543-937	adenylation domain
nMT	1030-1252	*N*-methyltransferase
PCP	1461-1528	Peptidyl-carrier protein
ORF 8	130	hypothetical protein
ORF 9	347	Substrate binding domain of ABC-type glycine betaine transport system
ORF 10	372	AA kinase domain; PUA - RNA-binding for translational machinery
ORF 11	303	Beta-lactamase superfamily domain
ORF 12	277	hypothetical protein
ORF 13	531	sugar-binding lipoprotein
ORF 14	294	putative ABC transporter permease protein
ORF 15	293	putative ABC transporter permease protein
ORF 16	143	four helix bundle protein; 23S rRNA-intervening sequence protein
ORF 17	395	ABC transporter ATP-binding protein

Module 1

Bioinformatic analysis of the gene sequence suggests that the initial core biosynthetic module, *hcaA*, encodes for the incorporation of a tyrosine residue. This module contains a condensation (C), adenylation (A), *O*-methyltransferase (oMT) and *N*-methyltransferase (nMT) as well as a peptidyl carrier protein (PCP) domain. The location of the *O*-methyltransferase and

the *N*-methyltransferase is consistent with the fact that the tyrosine is both *O*- and *N*-methylated in the hectoramide B structure. Initial inspection into the antiSMASH annotation of this module correctly identified A domain specificity for tyrosine. However, the annotations for the type of methyltransferase (MT) domains were not concurrent with our predictions. AntiSMASH predicted the presence of two nMT domains rather than the presence of at least one oMT domain and an nMT domain. Therefore, a phylogenetic tree of *O*-methyltransferase and *N*-methyltransferase domains from cyanobacteria was generated to elucidate the specificities of each of the annotated methyltransferase domains. **Figure 2.6** reveals that the first MT, hcaA-MT1 clades well with other oMT domains. More specifically, hca-MT1 has high sequence similarity to the oMT find on the *VatN* module of the vatiamide biosynthetic gene cluster (Moss et al., 2019). This oMT in the vatiamide BGC is also proposed to catalyze the methylation of the oxygen on the tyrosine residue. Furthermore, the second MT, hcaA-MT2, clades well with other nMT domains, specifically those within the hca pathway and the nMT of the *VatN* module in the vatiamide pathway.

In this module, hcaA, we propose that the A domain selects and activates a tyrosine residue. This is followed by methylation of the oxygen on the tyrosine by the oMT domain, then two methylations of the amine group of the tyrosine by a single nMT domain. This results in the incorporation of an *N,N*-dimethyl-*O*-methyltyrosine as the initiation unit of the NRPS.

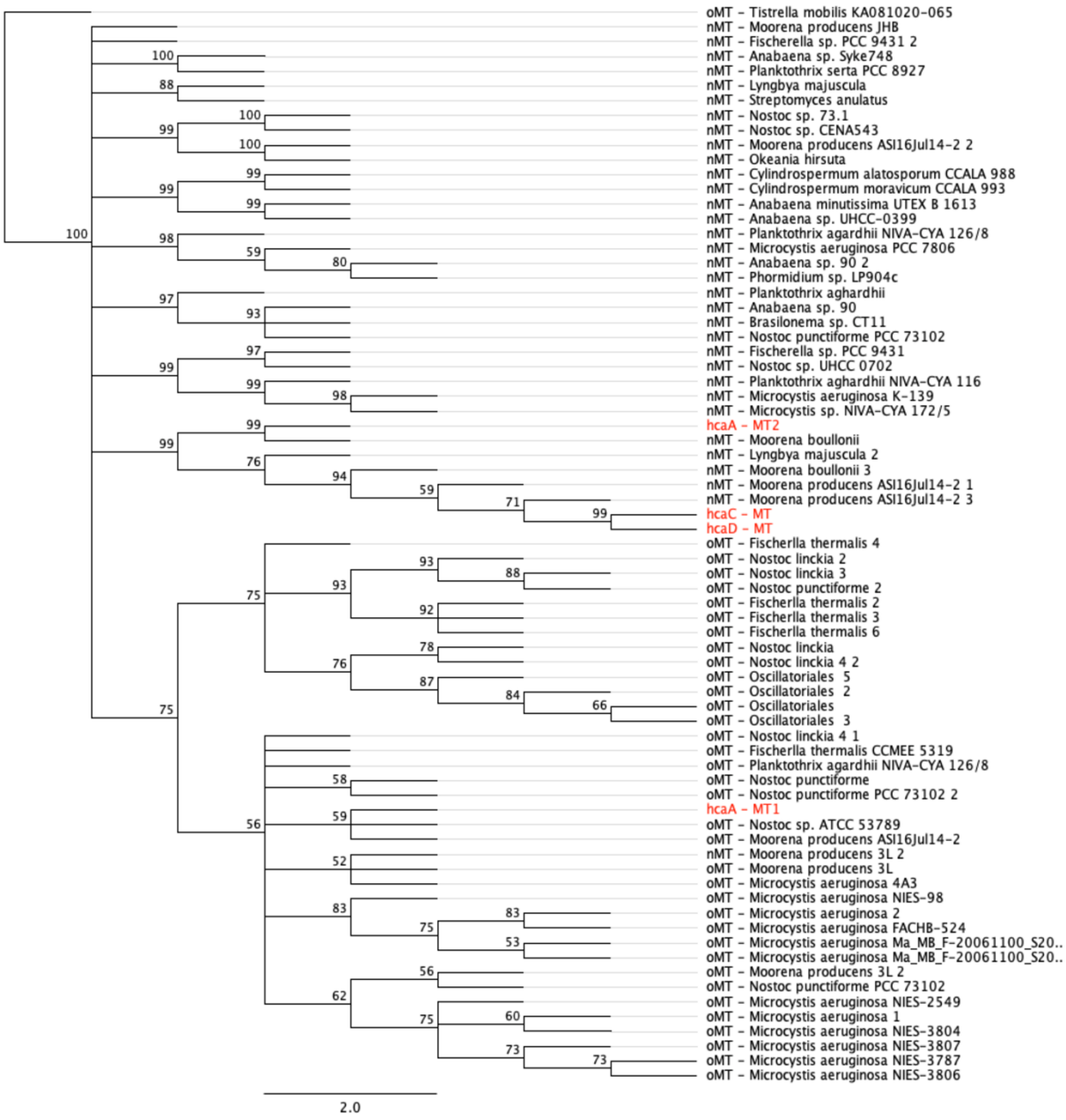

Figure 2.6 Phylogenetic tree of oxygen- and nitrogen-methyltransferase domains from Cyanobacteria
Bootstrap values, indicated at the nodes, were obtained from 100 replicates, and are reported as percentages. The scale bar corresponds to 2 nucleotide changes per site. Methyltransferase domains within the *hca* pathway are indicated in red.

Module 2

The second module, hcaB, is especially interesting because it is a non-ribosomal depsipeptide synthetase that codes for the incorporation of a 3-(4-methoxyphenyl)-2-oxopropanoic acid. Most known depsipeptides are cyclic in nature, so there is limited precedence of depsipeptide synthetases that produce linear nonribosomal depsipeptides. In depsipeptide modules that form the ester bond during elongation in noniterative synthesis, the A domain has selectivity for an α-keto acid substrate which is reduced to an α-hydroxy acid by a ketoreductase (KR) domain before incorporation into the chain (Alonso et. al, 2020). In the case of the depsipeptide synthetase module in the *hca* pathway, the proposed substrate for A domain selectivity is the α-keto acid version of tyrosine, 4-hydroxyphenylpyruvic acid. However, initial inspection into the substrate prediction from antiSMASH did not reach a consensus for substrate specificity. Additionally, there was not an annotation for an oMT domain that would install a methyl on the oxygen of the α-keto acid tyrosine. Therefore, a sequence and structural alignment of the hcaB-A domain (hcaB-A) with other NRPS A domains selecting for tyrosine and phenylalanine was generated to identify the specificity conferring residues of hcaB-A.

Interestingly, the proposed specificity conferring residues of hcaB-A did not coincide with previous patterns observed in α-keto acid selecting A domains. In depsipeptide A domains, the conserved Asp235 residue is typically substituted to an aliphatic residue while the remaining specificity conferring residues would match predicted amino acid selection (Alonzo & Schmeing, 2020). Thus, in the case of hcaB-A, we would expect the Asp235 residue to be substituted with an aliphatic residue, and the remaining specificity conferring residues to match those selecting for tyrosine. However, sequence analysis revealed that Asp235 was still present in hcaB-A, and the remaining proposed specificity conferring residues did not match those

expected for tyrosine (**Figure 2.7**). Furthermore, alignment of a structural model of hcaB-A and crystallography-derived structures of other NRPS A domains showed excellent congruence with the specificity conferring codes identified in the sequence alignment described above (**Fig. 2.7)**. Although it was expected that the specificity conferring codes would match those selecting for tyrosine, perhaps it could be explained by the absence of an annotated oMT domain in hcaB. As there was no annotation for an oMT domain, hcaB-A could be selecting for an α-keto acid *O*-methyl-tyrosine rather than an α-keto acid tyrosine. An additional methyl group on the oxygen of the α-keto acid tyrosine would alter the specificity binding pocket in order to accommodate this bulkier ligand. Additionally, although the Asp235 residue is typically substituted for an aliphatic residue in depsipeptide A domains, its presence in hcaB-A could play a role in α-keto acid selectivity. In a study investigating adenylation domain α-keto acid selection, Alonzo, and others (2020) suggests that an antiparallel carbonyl-carbonyl interaction between the α-keto group of the α-keto acid and carbonyl of glycine confers selectivity for α-keto acids. This antiparallel carbonyl-carbonyl interaction has the same strength of a hydrogen bond and was integral to α-keto acid selection (Alonzo et al., 2020). Based on the model of hcaB-A, Asp235 is positioned within 3.0 angstroms of the α-keto group of the α-keto *O*-methyl-tyrosine. This distance coincides with the bond distance of a hydrogen bond. This could explain why Asp235, which is normally substituted, is still present in hcaB-A.

The final mystery in this module is the annotated coenzyme A ligase (CAL) domain. The CAL domain is predicted to have specificity for a fatty acid. As there is no fatty acid moiety in the structure of hectoramide B, this domain is proposed to have no function in the biosynthesis of hectoramide B.

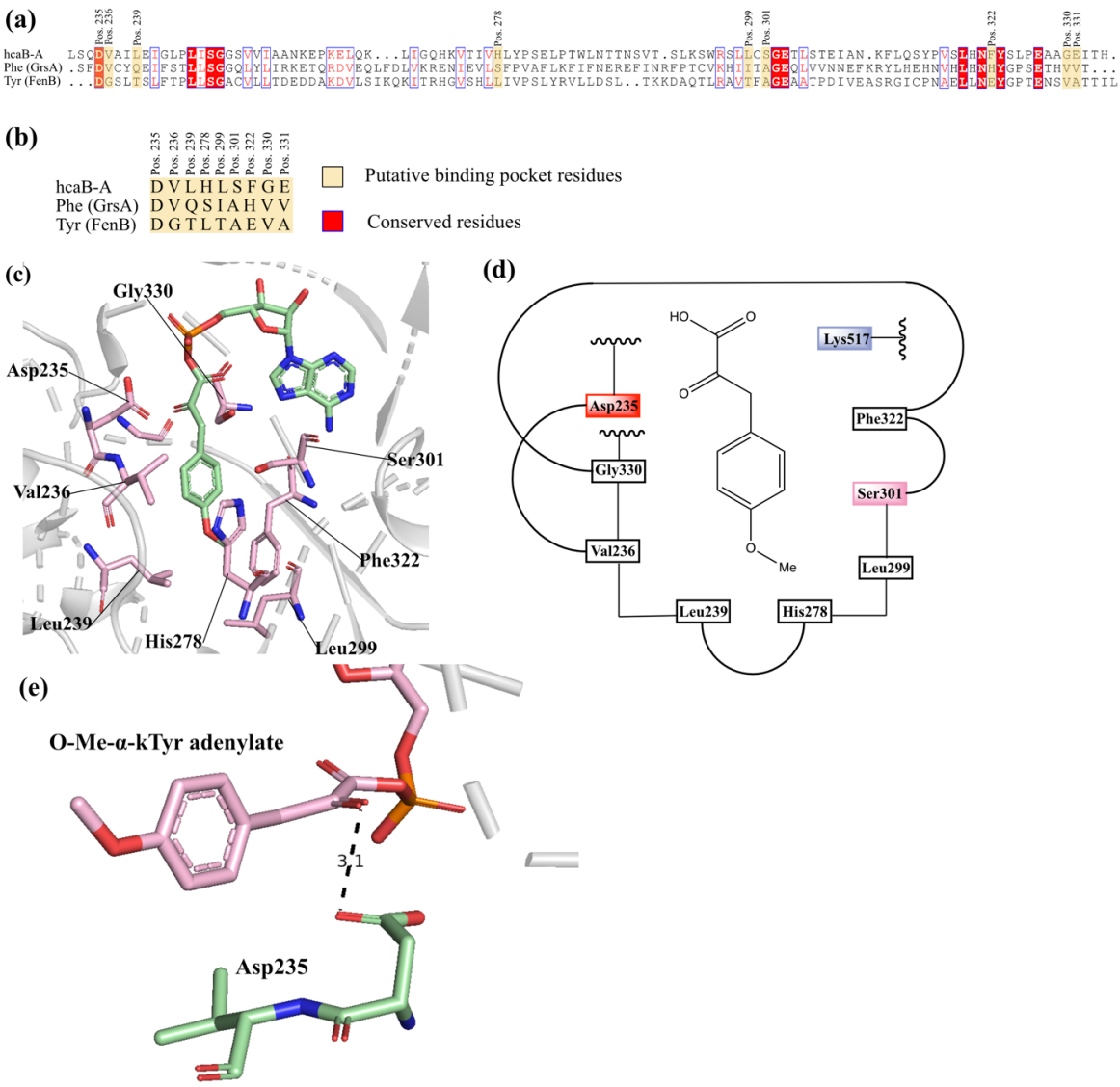

Figure 2.7 Sequence and Structural alignment of hcaB Adenylation domain reveals unique specificity conferring residues.

(a) Sequence alignment of primary sequence containing specificity conferring codes for adenylation (A) domains of hcaB-A, gramicidin S, and fengycin. Conserved residues are highlighted in red. Putative binding pocket residues are highlighted in yellow. (b) Putative binding pocket residues of hcaB-A. (c) Three-dimensional model of α-keto acid selecting hcaB-A domain generated using Alphafold2 bound to O-methyl-α-keto tyrosine (*O*-Me-α-kTyr) adenylate. The selectivity conferring residues (pink) are all within 5 Angstroms of the *O*-Me-α-kTyr ligand (pink). (d) Two-dimensional representation of the specificity pocket for *O*-methyl-α-keto tyrosine activating domain. (e) The α-keto group of the *O*-Me-α-kTyr (pink) binds through an antiparallel carbonyl-carbonyl interaction with the carbonyl group of Asp235.

We propose that after activation of α-keto *O*-methyl tyrosine by hcaB-A, the KR domain in this module reduces the α-keto acid to 2-hydroxy-3-(4-methoxyphenyl) propanoic acid

through an NADPH-dependent reaction. The C-domain then catalyzes the formation of the ester bond between the oxygen of the newly formed hydroxy group in this module 2 substrate and the carbonyl of the tyrosine from module 1.

Module 3

HcaC encodes for the incorporation of a *N*-methyl valine. Based on antiSMASH annotation, the A domain is predicted to incorporate a valine residue. Then, the nitrogen on the amine group of the valine is methylated by an *N*-methyltransferase domain. Lastly, the C domain catalyzes the condensation with the preceding dipeptide.

Module 4

The final module of HcaD is particularly unusual. The architecture of the module is similar to HcaC in that it is predicted to incorporate a *N*-methyl valine. However, sequence analysis reveals that the terminating thioesterase (TE) domain, which is required for release of the natural product, is absent. Canonical NRPS termination mechanisms involve TE-domain catalyzed hydrolysis or intramolecular cyclization that result in a free acid or lactone/lactam, respectively (McErlean et. al, 2019). Even so, terminal amide formation and chain release activity in terminal NRPS modules has been previously observed. For example, a terminal amide in an NRP has been found in dragonamide A, B and E, carmabin A, and vatiamide E and F (**Figure 2.7**). (Balunas et al., 2010; Hooper et al., 1998; Moss et al., 2019). More specifically, the VatR module in the vatiamide biosynthetic pathway was reported to produce vatiamide E and F, both of which contain a terminal amide. Although the mechanism and enzymology of termination is still unknown, it is theorized that there is an undescribed domain embedded in VatR, downstream of the PCP, that is responsible for the formation of the terminal amide (Moss

et. al, 2019). In the case of the hcaD, a similar motif may be present that gives rise to the formation of the terminal amide. Sequence alignment between this termination module, hcaD, and the VatR module in vatiamide E and F biosynthesis reveals a similarity of 72% (**Figure 2.8)**. Further exploration into both of these enzymatic domains can reveal what the precise mechanism of termination is in these modules.

In this module, we propose that the A domain selects for the incorporation of a valine residue. This is followed by methylation of the nitrogen group on the amine group by an *N*-methyltransferase domain. Then, there is condensation with the preceding tri-peptide. Lastly the complete hectoramide B is released from the *hca* pathway by an unknown mechanism.

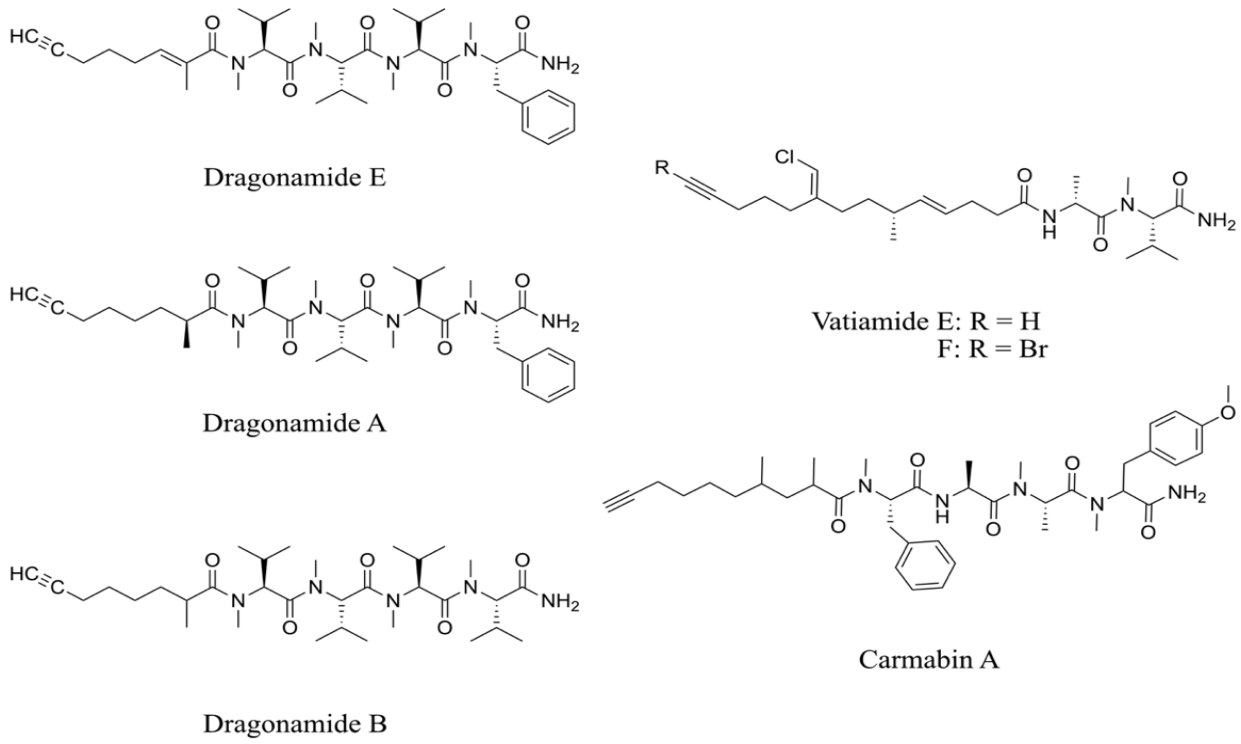

Figure 2.8 Five compounds with terminal amides, as of yet, with no known mechanisms for create the termination reaction.

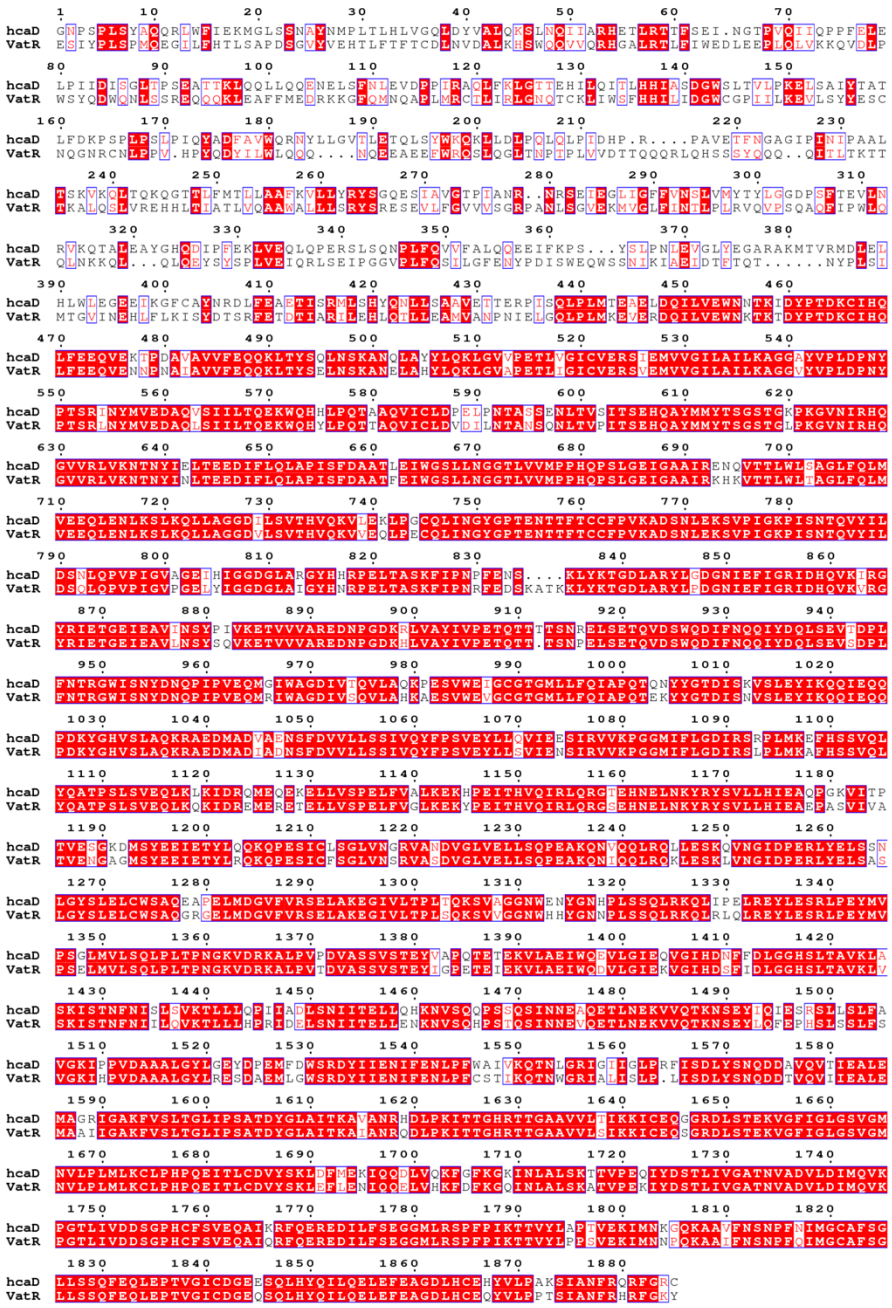

Protein	Amino acids	Proposed function
C	3-307	condensation domain
A	482-879	adenylation domain
nMT	973-1194	*N*-methyltransferase
PCP	1404-1470	Peptidyl-carrier protein
AD	1471-1885	Amidation domain

Figure 2.9 Sequence alignment of hcaD and vatR termination domains reveals 72% identity when aligning 1885 amino acids.

2.3.6 Antifungal susceptibility assay

To explore the antifungal properties of hectoramide B, a microbroth dilution method was employed. There were some technical difficulties that did not allow testing with the original strain of *C. albicans* used in the initial co-culture experiment. Therefore, *Saccharomyces cerevisiae* was used as a surrogate yeast strain instead. There was no antifungal activity at the testing range of up to 200 ug/mL for hectoramide B against *S. cerevisiae*.

2.4 Experimental Materials and Methods

2.4.1 General Experimental procedures

LR-LCMS data were obtained on a Thermo-Finnigan Survey Autosampler-Plus/MS-Pump-Plus/PDA-Plus Detector with Thermo Finnigan LCQ Advantage Max mass spectrometer. HPLC purification was carried out with Thermo Scientific Ultimate Dionex 3000 Pump/ RS Autosampler/ RS Diode Array detector/Automated Fraction Collector using Chromeleon v.7.2 software. All solvents were HPLC grade except for H20 which was purified with a Millipore Milli-Q system before use.

2.4.2 Microbial strains and culture conditions

M. producens JHB was collected from Hector Bay, Jamaica in 1996 and is maintained as a unialgal culture in our laboratory (Marquez et. al 2002). *Candida albicans* is stored in a -80^{o}C freezer in LB media with 20% glycerol. *Saccharomyces cerevisiae* is stored in a -80^{o}C freezer in LB media with 20% glycerol.

2.4.3 Optimization of media for *C. albicans* growth in SWBG11 media

LB-SWBG11 media preparation

LB media and SWBG11 media were prepared separately according to standard Gerwick lab protocols. Five combinations of LB-SWBG11 media were prepared at the following rations: 60:40% (LB:SWBG11), 40:60, 20:80, 10:90 and 100% LB media. For the initial round of acclimation to SWBG11 media, 30 mL of each type of media were aliquoted into a 50 mL Falcon tube. 1 mL of *C. albicans* in LB media was added to each tube and incubated for 24 hours at 37°C. Each combination was prepared in triplicate. For the second round of acclimation to SWBG11 media, 1 mL of *C. albicans* that was grown in 10:90 LB:SWBG11 media was added to 30mL of 10:90 LB-SWBG11 media and incubated for 24 hours at 37°C.

2.4.4 Co-culture, extraction, and isolation

A sample of *M. producens* JHB and 5 mL of *C. albicans* from LB-SWBG11 media prepared above was added to 125 mL of SWBG11 in a sterile, 250 mL plastic bottle. Similarly, JHB in 125 mL of SWBG11 medium, 5 mL of LB-SWBG11 *C. albicans* in 125 mL of SWBG11, and just 125 mL of SWBG11 media were prepared as background controls. Each of these four combinations were prepared in triplicate and cultivated at 27ºC and 756 Lux for 1 month. The bottles were sealed and opened weekly in a biosafety cabinet to facilitate adequate gas exchange.

2.4.5 Extraction, isolation, and characterization of HecB

Crude extract and LCMS

A 492.28 g wet sample of *M. producens* JHB, grown in laboratory culture as described above was extracted four times with 2:1 dichloromethane/methanol by sonication for 3 minutes followed by soaking for 15-20 min to afford 8.82 crude extract. A stock solution of the crude extract was prepared at 100 mg/mL in MeOH. Of the stock solution, 10ul (1 mg of crude extract) was diluted to 1 mg/mL in MeOH and filtered with C18 SPE column. Samples and a black of MeOH was run on Thermo Finnigan LCMS with a Phenomenex Kinetex 5µm C18 100 A 100 x 4.60 mm coumn. The elution used a gradient that began with 70% H2O (acidified with 1% v/v with HCOOH)/CH3CN (ACN) for 2 min, then ramped to 1% H2O/CH3CN at 22 min, held there for 4 min, then brought back to 70% at 28 min, and re-equilibrated for 4 min.

VLC and HPLC purification

The crude extract was preoperatively fractionated by Vacuum Liquid Chromatography (VLC) by standard Gerwick laboratory protocol. Fixed volumes of progressively polar mixtures of hexanes-EtOAc-MeOH proportional to the size of the extraction were prepared (Nine fractions: 100% hexanes, 10% EtOAc/hexanes, 20% EtOAc/hexanes, then 20% increments to 100% EtOAc, 25% MeOH/EtOAc, and 100% MeOH). The 4.05 g of crude extract was solubilized in 4 mL of 2:1 DCM/MeOH and mixed in a 500 mL round bottom flask with 16.2 g of TLC grade silica. The mixture was dried and loaded onto the column for VLC.

The VLC fractions containing hectoramide B (25% MeOH/EtOAc and 100% MeOH) were combined and resolubilized in 100 mL of EtOAc for liquid-liquid extraction with H_2O. Three iterations of liquid-liquid extraction were performed in a separatory funnel to remove salts

from the extract and the organic layer was retained to afford 0.5253 g of Fraction HI. Fr. HI was further purified by HPLC using a Phenomenex Kinetex 5 μm C18 100A LC 150 x 21.2 mm column and gradient elution using 20% CH_3CN/H_2O with 1% formic acid at the flow rate of 9 mL/min, which yielded 6 subfractions. Fraction HI #3 contained hectoramide B and was purified further using Phenomenex Kinetex 5 μm C18 100 A LC 100 x 4.60 mm column and gradient elution using 20% CH_3CN/H_2O with 1% formic acid at the flow rate of 1 mL/min to afford 16.5 mg of hectoramide B.

2.4.6 DNA isolation

DNA from *M. producens* JHB was obtained using "QIAGEN Bacterial Genomic Extraction Kit". High molecular weight DNA was extracted using method as described in Leao and others (2017) (Leao et. al 2017).

2.4.7 Genome sequencing, QC, and assembly

Data generation was conducted using Oxford Nanopore PromethION sequencing platform by UC Davis Genomics Core. SQK-LSK110 and FLO-PRO002 were used for library construction and data generation. All data generation process was conducted by following the protocols from the manufacturer. Base-calling was conducted using Guppy v5.0.7 with dna_r9.4.1_450bps_hac model. A subset of the sequencing read data was generated with Filtlong v.0.2.1 with parameters Min_length=2000, keep-percent=90, and target_bases=1500000000 for read filtering.

Two long-read assembly tools (Unicycler v.0.5.0 and Flye v.2.9) which can conduct assembly using only nanopore reads or with the addition of illumina reads were used for this study. Flye was used for assembly using only nanopore reads with genome-size=9m as a

parameter (Kolmogorov et al., 2019). Unicycler was used for assembly using only nanopore reads and combination with illumina reads with default parameters for hybrid assembly and long-read only assembly (Wick et al., 2017). Unicycler is a genome assembly workflow that utilizes SPades, Racon, and Pilon as part of the workflow. Metagenome binning was conducted using Metabat2 v.2.15 with default parameters (Kang et al., 2019). The bins were annotated using Checkm v.1.2.0 with taxonomy workflow, rank=phylum, and taxon=Cyanobacteria as the parameters (Parks et al., 2015).

2.4.8 Genome polishing and assessment

Short reads from previous Illumina sequencing were mapped to assembly using bwa-mem2 v.0.7.17 and polishing was conducted using Pilon v.1.24 with default parameters. 3 iterations of polishing were performed (Li et al., 2009; Walker et al., 2014).

For polished genome evaluation, BUSCOv5.3.2 was used with cyanobacteria_odb10 database. N50, contig number, and genome lengths were identified using Quast v.5.0.2 using default parameters (Gurevich et al., 2013; Manni et al., 2021). To assess BGC content, Antismash v.6.0 was used on the web-based platform with settings detection=relaxed, and all extra features turned on (Blin et al., 2021). The resulting region that contained the hectoramide B BGC was downloaded as Genbank file and further investigated using Geneious Prime v.2022.1.1.

2.4.9 Sequence alignments and Phylogenetic tree

Sequence alignments were generated using Clustal Omega v. 1.2.3 on Geneious prime software with default parameters. Methyltransferase domain sequences were obtained from NCBI and MiBIG database (Kautsar et al., 2020). Phylogenetic tree was generated using

Geneious Tree Builder with Jukes-Cantor model and default parameters. The domains used in phylogenetic tree generation are listed in **Table 2.x.** An oxygen methyltransferase from *Tistrella mobilis* KA091020-065 was used as the outgroup. Sequence alignment figures were generated by Espript 3.0 (Roberet and Gouet, 2014).

Table 2.3 Methyltransferase domains from cyanobacteria used to build Phylogenetic tree. Sequences were prepared from NCBI database and MiBIG database.

Organism	Specificity	Genbank accession ID	MIBIG Accession ID	Natural product	Gene
Anabaena minutissima UTEX B 1613	nMT	MH325199.1	BGC0001952	minutissamide A	puwA
Anabaena sp. 90	nMT	GU174493.1	BGC0000302	Anabaenopeptin	aptC
Anabaena sp. 90	nMT	AY212249.1	BGC0001016	microcystin	mycA
Anabaena sp. Syke748	nMT	KJ502174.1	BGC0000369	hassalidin C	hasY
Anabaena sp. UHCC-0399	nMT	MH325200.1	BGC0001953	puwainaphycin F	puwA
Brasilonema sp. CT11	nMT	MT670293.1	BGC0002512	Anabaenopeptin 788	aptC
Cylindrospermum alatosporum CCALA 988	nMT	KM078884.1	BGC0001125	puwainaphycin A	puwA
Cylindrospermum moravicum CCALA 993	nMT	MH325197.1	BGC0001950	puwainaphycin F	puwA
Fischerella sp. PCC 9431	nMT	NZ_KE650771.1	BGC0001467	hapalosin	FIS9431_RS32925
Fischerella sp. PCC 9431	nMT	NZ_KE650771.1	BGC0002624	fischerazole A	FIS9431_RS33740
Fischerella thermalis	oMT	WP_102182194.1	-	-	-
Fischerella thermalis	oMT	WP_102176734.1	-	-	-
Fischerella thermalis	oMT	WP_102172701.1	-	-	-
Fischerella thermalis	oMT	WP_009460361.1	-	-	-
Fischerella thermalis	oMT	PMB16080.1	-	-	-
Lyngbya majuscula	nMT	AY588942.1	BGC0000384	lyngbyatoxin	LtxA
Lyngbya majuscula	nMT	AF516145.1	BGC0000962	barbamide	barG
Microcystis aeruginosa	oMT	WP_002738215.1	-	-	-
Microcystis aeruginosa	oMT	TRU39906.1	-	-	-
Microcystis aeruginosa	oMT	TRU37805.1	-	-	-
Microcystis aeruginosa	oMT	ROI01679.1	-	-	-
Microcystis aeruginosa	oMT	ODV39796.1	-	-	-
Microcystis aeruginosa	oMT	GCL56935.1	-	-	-
Microcystis aeruginosa	oMT	GCL53376.1	-	-	-
Microcystis aeruginosa	oMT	GCL49408.1	-	-	-
Microcystis aeruginosa	oMT	GCL44916.1	-	-	-
Microcystis aeruginosa	oMT	BCU10658.1	-	-	-
Microcystis aeruginosa	oMT	AZP89422.1	-	-	-
Microcystis aeruginosa	oMT	AKE63547.1	-	-	-
Microcystis aeruginosa K-139	nMT	AB481215.1	BGC0001018	micropeptin K139	mcnC
Microcystis aeruginosa PCC 7806	nMT	AF183408.1	BGC0001017	microcystin LR	mycA
Microcystis sp. NIVA-CYA 172/5	nMT	DQ075244.1	BGC0000332	Cyanopeptolin	mcnC
Moorea producens JHB	nMT	KY315923.1	BGC0001560	Cryptomaldamide	cpmB
Moorena bouillonii	nMT	GA0081470	-	-	-
Moorena producens	nMT	OLT68856.1	-	-	-
Moorena producens 3L	oMT	EGJ32162.1	-	-	-
Moorena producens 3L	oMT	EGJ32090.1	-	-	-
Moorena producens ASI16Jul14-2	nMT	MK618714.1	BGC0002296	Vatiamide A,B	VatN - MT1
Moorena producens ASI16Jul14-2	oMT	MK618714.1	BGC0002296	Vatiamide A,B	VatN - MT2
Moorena producens ASI16Jul14-2	nMT	MK618714.1	BGC0002296	Vatiamide A,B	VatR
Moorena producens ASI16Jul14-2	nMT	MK618714.1	BGC0002296	Vatiamide A,B	VatS
Nostoc linckia	oMT	WP_242052790.1	-	-	-
Nostoc linckia	oMT	WP_190659225.1	-	-	-
Nostoc linckia	oMT	WP_099068175.1	-	-	-
Nostoc linckia	oMT	WP_096540073.1	-	-	-
Nostoc linckia	oMT	WP_096538766.1	-	-	-
Nostoc punctiforme	oMT	WP_190950119.1	-	-	-
Nostoc punctiforme	oMT	WP_190948102.1	-	-	-
Nostoc punctiforme	oMT	ACC83904.1	-	-	-
Nostoc punctiforme	oMT	ACC82073.1	-	-	-
Nostoc punctiforme PCC 73102	nMT	CP001037.1	BGC0001479	Anabaenopeptin NZ857, nostamide A	Npun_F2462
Nostoc sp. 73.1	nMT	JF342711.1	BGC0000396	nodularin	ndaA
Nostoc sp. ATCC 53789	oMT	EF159954.1	BGC0000975	cryptophycin-327	crpC
Nostoc sp. CENA543	nMT	MF668122.1	BGC0001705	nodularin	ndaA
Nostoc sp. UHCC 0702	nMT	CP071065.1	BGC0002572	heinamide A1	JYQ62_16355
Okeania hirsuta	nMT	MK142793.1	BGC0001971	Malyngamide I	MgcJ
Oscillatoriales	oMT	TAG39103.1	-	-	-
Oscillatoriales	oMT	TAF21875.1	-	-	-
Oscillatoriales	oMT	TAE13988.1	-	-	-
Oscillatoriales cyanobacterium	oMT	TAE67097.1	-	-	-
Phormidium sp. LP904c	nMT	MK870090.1	BGC0002297	MC-LR	mycA
Planktothrix agardhii	oMT	CAD29800.2	-	-	-
Planktothrix agardhii NIVA-CYA 126/8	nMT	AJ441056.1	BGC0001015	microcystin	mycA
Planktothrix aghardhii	nMT	EF672686.1	BGC0000301	Anabaenopeptin 908	apnC
Planktothrix aghardhii NIVA-CYA 116	nMT	DQ837301.1	BGC0000331	Cyanopeptolin	ociB
Planktothrix serta PCC 8927	nMT	LT546031.1	BGC0001614	hassalidin E	hasY
Streptomyces anulatus	nMT	HM038106.1	BGC0000296	actinomycin D	acmC
Tistrella mobilis KA081020-065	oMT	CP003239.1	BGC0000985	didemnin	didJ

Table 2.4 Adenylation domains used for sequence and structural alignment with hcaB adenylation domain

Domain name	Specificity	Organism	Genbank accession number	MiBIG accession number	Natural Product	PDB accession code
FenB	Tyrosine	*Bacillus velezensis FZB42*	CP000560.1	BGC0001095	fengycin	-
GrsA	Phenylalanine	*Aneurinibacillus migulanus*	LGUG01000004.1	BGC0002122	gramicidin S	-
LgrA (mutant)	α-ketoisocaproic acid	*Brevibacillus parabrevis*	-	-	Linear gramicidin	6ULZ

2.4.10 Structural model and alignment

The model of the hcaB adenylation domain was built using AlphaFold2 and was analyzed in PyMol v.2.0 (Jumper et al., 2021; Schrödinger, LLC, 2015). The model was superimposed onto other A domains from PDB database to obtain structural alignments (Table 2.4). The residues on the hcaB model within 5 Angstroms of ligand from A domain structures were selected and interrogated for identification of predicted binding site residues.

2.4.11 Antifungal Susceptibility Assay

Minimum inhibitory concentrations (MIC) were determined using microtiter broth dilution in Yeast Peptone Dextrose (YPD) media. Frozen spore suspensions of *Saccharomyces cerevisiae* were grown on an overnight plate culture in YPD agar. Wells were inoculated to a final concentration of 1.5×10^5 cfu/mL. Plates were incubated at 30 C for 20 hours and the MICs were defined as the lowest concentration of drug completely inhibiting visible growth. Cycloheximide and Fluconazole were used as positive controls.

2.5 References

Alonzo, D. A., Chiche-Lapierre, C., Tarry, M. J., Wang, J., & Schmeing, T. M. (2020). Structural basis of keto acid utilization in nonribosomal depsipeptide synthesis. *Nature Chemical Biology*, *16*(5), 493–496. https://doi.org/10.1038/s41589-020-0481-5

Alonzo, D. A., & Schmeing, T. M. (2020). Biosynthesis of depsipeptides, or Depsi: The peptides with varied generations. *Protein Science : A Publication of the Protein Society*, *29*(12), 2316–2347. https://doi.org/10.1002/pro.3979

Balunas, M. J., Linington, R. G., Tidgewell, K., Fenner, A. M., Ureña, L.-D., Togna, G. D., Kyle, D. E., & Gerwick, W. H. (2010). Dragonamide E, a Modified Linear Lipopeptide from Lyngbya majuscula with Antileishmanial Activity. *Journal of Natural Products*, *73*(1), 60–66. https://doi.org/10.1021/np900622m

Blin, K., Shaw, S., Kloosterman, A. M., Charlop-Powers, Z., van Wezel, G. P., Medema, M. H., & Weber, T. (2021). antiSMASH 6.0: Improving cluster detection and comparison capabilities. *Nucleic Acids Research*, *49*(W1), W29–W35. https://doi.org/10.1093/nar/gkab335

Boudreau, P. D., Monroe, E. A., Mehrotra, S., Desfor, S., Korobeynikov, A., Sherman, D. H., Murray, T. F., Gerwick, L., Dorrestein, P. C., & Gerwick, W. H. (2015). Expanding the Described Metabolome of the Marine Cyanobacterium Moorea producens JHB through Orthogonal Natural Products Workflows. *PLOS ONE*, *10*(7), e0133297. https://doi.org/10.1371/journal.pone.0133297

Dong-Chan Oh, Christopher A. Kauffman, Paul R. Jensen, and, & Fenical*, W. (2007, February 27). *Induced Production of Emericellamides A and B from the Marine-Derived Fungus Emericella sp. In Competing Co-culture* (world) [Review-article]. ACS Publications; American Chemical Society. https://doi.org/10.1021/np060381f

Edwards, D. J., Marquez, B. L., Nogle, L. M., McPhail, K., Goeger, D. E., Roberts, M. A., & Gerwick, W. H. (2004). Structure and Biosynthesis of the Jamaicamides, New Mixed Polyketide-Peptide Neurotoxins from the Marine Cyanobacterium Lyngbya majuscula. *Chemistry & Biology*, *11*(6), 817–833. https://doi.org/10.1016/j.chembiol.2004.03.030

Engene, N., Rottacker, E. C., Kaštovský, J., Byrum, T., Choi, H., Ellisman, M. H., Komárek, J., & Gerwick, W. H. Y. 2012. (n.d.). Moorea producens gen. Nov., sp. Nov. And Moorea bouillonii comb. Nov., tropical marine cyanobacteria rich in bioactive secondary metabolites. *International Journal of Systematic and Evolutionary Microbiology*, *62*(Pt_5), 1171–1178. https://doi.org/10.1099/ijs.0.033761-0

Gerwick, W. H., Proteau, P. J., Nagle, D. G., Hamel, E., Blokhin, A., & Slate, D. L. (1994). Structure of Curacin A, a Novel Antimitotic, Antiproliferative and Brine Shrimp Toxic Natural Product from the Marine Cyanobacterium Lyngbya majuscula. *The Journal of Organic Chemistry*, *59*(6), 1243–1245. https://doi.org/10.1021/jo00085a006

Guinea, J. (2014). Global trends in the distribution of Candida species causing candidemia. *Clinical Microbiology and Infection*, *20*, 5–10. https://doi.org/10.1111/1469-0691.12539
Gurevich, A., Saveliev, V., Vyahhi, N., & Tesler, G. (2013). QUAST: Quality assessment tool for genome assemblies. *Bioinformatics*, *29*(8), 1072–1075. https://doi.org/10.1093/bioinformatics/btt086

Hooper, G. J., Orjala, J., Schatzman, R. C., & Gerwick, W. H. (1998). Carmabins A and B, New Lipopeptides from the Caribbean Cyanobacterium Lyngbya majuscula. *Journal of Natural Products*, *61*(4), 529–533. https://doi.org/10.1021/np970443p

Jumper, J., Evans, R., Pritzel, A., Green, T., Figurnov, M., Ronneberger, O., Tunyasuvunakool, K., Bates, R., Žídek, A., Potapenko, A., Bridgland, A., Meyer, C., Kohl, S. A. A., Ballard, A. J., Cowie, A., Romera-Paredes, B., Nikolov, S., Jain, R., Adler, J., … Hassabis, D. (2021). Highly accurate protein structure prediction with AlphaFold. *Nature*, *596*(7873), Article 7873. https://doi.org/10.1038/s41586-021-03819-2

Kabir, M. A., Hussain, M. A., & Ahmad, Z. (2012). Candida albicans: A Model Organism for Studying Fungal Pathogens. *ISRN Microbiology*, *2012*, 538694. https://doi.org/10.5402/2012/538694

Kang, D. D., Li, F., Kirton, E., Thomas, A., Egan, R., An, H., & Wang, Z. (2019). MetaBAT 2: An adaptive binning algorithm for robust and efficient genome reconstruction from metagenome assemblies. *PeerJ*, *7*, e7359. https://doi.org/10.7717/peerj.7359

Kautsar, S. A., Blin, K., Shaw, S., Navarro-Muñoz, J. C., Terlouw, B. R., van der Hooft, J. J. J., van Santen, J. A., Tracanna, V., Suarez Duran, H. G., Pascal Andreu, V., Selem-Mojica, N., Alanjary, M., Robinson, S. L., Lund, G., Epstein, S. C., Sisto, A. C., Charkoudian, L. K., Collemare, J., Linington, R. G., … Medema, M. H. (2020). MIBiG 2.0: A repository for biosynthetic gene clusters of known function. *Nucleic Acids Research*, *48*(D1), D454–D458. https://doi.org/10.1093/nar/gkz882

Kolmogorov, M., Yuan, J., Lin, Y., & Pevzner, P. A. (2019). Assembly of long, error-prone reads using repeat graphs. *Nature Biotechnology*, *37*(5), Article 5. https://doi.org/10.1038/s41587-019-0072-8

Leao, T., Castelão, G., Korobeynikov, A., Monroe, E. A., Podell, S., Glukhov, E., Allen, E. E., Gerwick, W. H., & Gerwick, L. (2017). Comparative genomics uncovers the prolific and distinctive metabolic potential of the cyanobacterial genus Moorea. *Proceedings of the National Academy of Sciences of the United States of America*, *114*(12), 3198–3203. https://doi.org/10.1073/pnas.1618556114

Li, H., Handsaker, B., Wysoker, A., Fennell, T., Ruan, J., Homer, N., Marth, G., Abecasis, G., Durbin, R., & 1000 Genome Project Data Processing Subgroup. (2009). The Sequence Alignment/Map format and SAMtools. *Bioinformatics*, *25*(16), 2078–2079. https://doi.org/10.1093/bioinformatics/btp352

Liu, Y., Law, B. K., & Luesch, H. (2009). Apratoxin A Reversibly Inhibits the Secretory Pathway by Preventing Cotranslational Translocation. *Molecular Pharmacology*, *76*(1), 91–104. https://doi.org/10.1124/mol.109.056085

Lockhart, S. R. (2014). Current Epidemiology of Candida Infection. *Clinical Microbiology Newsletter*, *36*(17), 131–136. https://doi.org/10.1016/j.clinmicnews.2014.08.001
Logsdon, G. A., Vollger, M. R., & Eichler, E. E. (2020). Long-read human genome sequencing and its applications. *Nature Reviews Genetics*, *21*(10), Article 10. https://doi.org/10.1038/s41576-020-0236-x

Luesch, H., Yoshida, W. Y., Moore, R. E., Paul, V. J., & Corbett, T. H. (2001). Total Structure Determination of Apratoxin A, a Potent Novel Cytotoxin from the Marine Cyanobacterium *Lyngbya m ajuscula*. *Journal of the American Chemical Society*, *123*(23), 5418–5423. https://doi.org/10.1021/ja010453j

Manni, M., Berkeley, M. R., Seppey, M., Simão, F. A., & Zdobnov, E. M. (2021). BUSCO Update: Novel and Streamlined Workflows along with Broader and Deeper Phylogenetic Coverage for Scoring of Eukaryotic, Prokaryotic, and Viral Genomes. *Molecular Biology and Evolution*, *38*(10), 4647–4654. https://doi.org/10.1093/molbev/msab199

Marquez, B. L., Watts, K. S., Yokochi, A., Roberts, M. A., Verdier-Pinard, P., Jimenez, J. I., Hamel, E., Scheuer, P. J., & Gerwick, W. H. (2002). Structure and Absolute Stereochemistry of Hectochlorin, a Potent Stimulator of Actin Assembly. *Journal of Natural Products*, *65*(6), 866–871. https://doi.org/10.1021/np0106283

Moss, N. A., Seiler, G., Leão, T. F., Castro-Falcón, G., Gerwick, L., Hughes, C. C., & Gerwick, W. H. (2019). Nature's combinatorial biosynthesis produces vatiamides A-F. *Angewandte Chemie (International Ed. in English)*, *58*(27), 9027–9031. https://doi.org/10.1002/anie.201902571

Paatero, A. O., Kellosalo, J., Dunyak, B. M., Almaliti, J., Gestwicki, J. E., Gerwick, W. H., Taunton, J., & Paavilainen, V. O. (2016). Apratoxin Kills Cells by Direct Blockade of the Sec61 Protein Translocation Channel. *Cell Chemical Biology*, *23*(5), 561–566. https://doi.org/10.1016/j.chembiol.2016.04.008

Parks, D. H., Imelfort, M., Skennerton, C. T., Hugenholtz, P., & Tyson, G. W. (2015). CheckM: Assessing the quality of microbial genomes recovered from isolates, single cells, and metagenomes. *Genome Research*, *25*(7), 1043–1055. https://doi.org/10.1101/gr.186072.114

Robert, X. and Gouet, P. (2014) "Deciphering key features in protein structures with the new ENDscript server". *Nucl. Acids Res*. **42**(W1), W320-W324 - doi: 10.1093/nar/gku316 (**freely accessible online**).

Schrödinger, LLC. (2015). *The PyMOL Molecular Graphics System, Version 1.8*.
Walker, B. J., Abeel, T., Shea, T., Priest, M., Abouelliel, A., Sakthikumar, S., Cuomo, C. A., Zeng, Q., Wortman, J., Young, S. K., & Earl, A. M. (2014). Pilon: An Integrated Tool for

Comprehensive Microbial Variant Detection and Genome Assembly Improvement. *PLOS ONE*, *9*(11), e112963. https://doi.org/10.1371/journal.pone.0112963

Wick, R. R., Judd, L. M., Gorrie, C. L., & Holt, K. E. (2017). Unicycler: Resolving bacterial genome assemblies from short and long sequencing reads. *PLOS Computational Biology*, *13*(6), e1005595. https://doi.org/10.1371/journal.pcbi.1005595

2.6 Acknowledgements

Chapter 2, in full, is currently being prepared for publication. Ngo, Thuan-Ethan; Guild, Rory; Ecker, Andrew; Naman, Ben; Alexander, Kelsey; Gerwick, Lena; Gerwick, William. "Induced production and Biosynthesis of Novel Linear Depsipeptide Hectoramide B, from Marine Cyanobacterium Moorena producens JHB in Competing Co-culture". The thesis author was the primary investigator and author of this paper.

I'd also like to recognize Dr. Ruta Sahasrabudhe who assisted in the sequencing that was carried out by the DNA Technologies and Expression Analysis Core at the UC Davis Genome Center, supported by NIH Shared Instrumentation Grant 1S10OD010786-01. I'd also like thank Dr. Vikram Shende and Andrew Ecker on their assistance with the generation of structural data of hcaB adenylation domain.

Chapter 3: Development and Optimization of Cryopreservation Method for Tropical Marine Cyanobacteria

3.1 Abstract

Cryopreservation is a valuable method for the long-term preservation of organic materials including life forms by cooling them down to ultralow temperatures. This method has been successfully applied to many species of cyanobacteria, however, cyanobacteria with larger cell sizes and filamentous strains have appeared to be recalcitrant to cryopreservation. Therefore, in this study, we sought to optimize and develop methods for cryopreservation of several filamentous strains of cyanobacteria that are part of the Gerwick lab collection. We were able to successfully cryopreserve some species of the genus *Leptolyngbya*, *Oscillatoria*, and *Moorena*. Other species showed some capability to be cryopreserved, however, further optimization will need to be conducted in order to successfully cryopreserve them.

3.2 Introduction

Cryopreservation is a method used to preserve cells, tissues, and other organic materials by cooling them down to ultralow temperatures. This method has many applications in the medical field, food sciences, and preservation of cells or organs. For example, cryopreservation can be used to store and preserve spermatozoa and oocytes for artificial insemination (Jang et al., 2017). In fact, in 1949, human spermatozoa were successfully cryopreserved and recovered using glycerol as a cryoprotective agent (Pegg, 2007). Since then, many studies have been conducted to optimize cryopreservation for a variety of cell types from different organisms

Cyanobacteria are routinely maintained through serial subculturing. Over a long period of time, serial subculturing can be labor-intensive for larger algal collections, genetic changes may

occur, and subsequently phenotypic changes may be observed. This is especially costly to the natural products field where we rely on these cyanobacteria to have a specific metabolic profile that we want to explore over a period of years. Therefore, cryopreservation is an ideal method for the long-term storage of these precious cultures. Many different species of cyanobacteria have been successful cryopreserved with high post-thaw viability. Algal collections around the world such as The Culture Collection of Algae at the University of Texas at Austin (UTEX) (USA) have observed great success in cryopreserving chlorarachniophytes, eustigmatophytes, pelagophytes, phaeothamniophytes, and ulvophytes cyanobacteria. However, many cyanobacteria with larger cell sizes, and most filamentous strains, are recalcitrant to cryopreservation (Day, 2007). The Gerwick lab algal collection mostly consists of tropical, filamentous cyanobacteria that have been difficult to store using cryopreservation. Therefore, we sought to optimize a cryopreservation method for several of our cyanobacteria cultures including species from the genus *Moorena*, *Leptolyngbya*, *Spirulina*, and others.

3.2.1 General factors to consider with cryopreservation

There are several factors to consider when developing the most optimal method for cryopreservation because they will have an effect on intracellular ice formation and subsequently recovery of cells post-cryopreservation. Intracellular ice formation can cause rupturing of cells and is largely dependent on osmolality, or solute concentration, during the cryopreservation process (Pegg, 2007). Improper selection of the temperature change rate during cooling and warming and cryoprotective agent (CPA) can install barriers to successful growth recovery.

During cooling, salt concentration increases which causes cells to become dehydrated and water to leave the cells. Slow-rate freezing can allow for ample time for water to leave the cells,

however, if the rate is too slow, ice crystals can form before the cells are dehydrated. On the other hand, rapid-rate freezing can allow for the ice to reach a vitrified, or glass-like state, which prevents the nucleation of ice. However, if the rate is not quick enough, ice crystals can form before the cells are dehydrated. A delicate balance needs to be achieved to ensure post-thaw viability. Similarly, during warming or post-thaw, the rate of warming needs to be optimized to prevent further cryo-injury. With slow-rate warming, ice crystals can reform, causing injury to the cells, however, a longer exposure time can also prevent major swelling of the cells from osmotic uptake. On the other hand, rapid-rate cooling can eliminate ice crystals quickly, thereby reducing ice crystal damage. However, rapid swelling of the cells can occur during osmotic uptake which will make the cells burst and die.

An appropriate CPA needs to be selected otherwise toxicity can occur to the cells. CPAs are used in cryopreservation because they depress the freezing point of water, allowing more time for intracellular water effusion (Pegg, 2007). There can either be penetrative or non-penetrative CPAs. Penetrative CPAs (pCPAs) are small enough to cross through the cell membrane whereas non-penetrative CPAs are larger and affect extracellular osmolality. In high concentrations, CPAs can be toxic to cells and cause damage whereas in lower concentrations, the CPA will not depress of the freezing point of water which will lead to ice crystal formation. Non-penetrating CPAs (npCPA) work by balancing the osmolality of extracellular solutes. NpCPAs, like proline, are naturally occurring molecules within the cell. Therefore, by introducing them extracellularly, you can control the efflux of water out of the cell and thereby avoid cell shrinkage. Some examples of commonly used CPAs include: dimethylsulfoxide (DMSO), methanol (MeOH), and glycerol. Post-thaw cell viability largely depends on all these carefully selected parameters.

Previous attempts have been made to cryopreserve the cyanobacterial cultures in the Gerwick lab collection. However, many of the different species have been recalcitrant to cryopreservation. Therefore, in this work, we sought to optimize and tailor specific cryopreservation protocols for the long-term storage of marine cyanobacteria of the Gerwick lab algal collection.

3.3 Experimental Materials and Methods

3.3.1 Cyanobacterial strains used for Cryopreservation

All cultures are maintained with SWBG11 media in a 28°C controlled temperature room with a 16 hr light/8 hr dark cycle. The collection locations, cell parameters, and associated metabolites are listed in **Table 3.1**.

Table 3.1 Collection data for cyanobacterial specimens used in this study

Collection Tag	Cells parameters, um	Genus/Family	Location	Collection GPS coordinates		Depth (m)	Metabolites
				Latitude	Longitude		
ASX22JUL14-2a (ASX)	leptolyngbya with a few unicells; emerald green pufs, balls of fur	*Leptolyngbya*	American Samoa	N/A	N/A		N/A
ISB3NOV94-8A (ISB)	L=3-5 um, W=1.5 um, dark purple with black and grey puffs	*Leptolyngbya*	Sulawesi, Indonesia	1°51'50.7"S	120°34'51.4"E		Leptochelin, Apratoxins, Phormidolide
ASY22JUL14-1 (ASY)	L=8 um, W=60 um; black 'hair' moorena	*Moorena*	American Samoa	N/A	N/A		N/A
GFR15JUN17-1.1 (GFR)	brown, good, filaments	*Moorena bouillonii*	Guam	N/A	N/A		N/A
PNG19MAY05-8 (PNG)	red-brown hair-like filaments	*Moorena bouillonii*	Pigeon Island, Papau New Guinea	4°16.063"S	152°20.266"E	10m	Apratoxin A-C; Cyanolide A; Lyngbyabellin
JHB22AUG96-1 (JHB)	L=18 um, W=100 um, dark green hair-like filaments	*Moorena producens*	Hector Bay, Jamaica	18°09'01.8"N	77°18'10.6"W	2m	Hectochlorin; Jamaicamides A-C; Cryptomaldamide; Hectoramide B
PAL15AUG08-1 (PAL)	L=15 um, W=60-90 um black-green 'hair'	*Moorena producens*	Strawn Island, Palmyra	05′52.172N,	162′05.047W	<1 m	Malyngamide C, Curacin D, Palmyramide A, honuaiakeamide A
3L-Oscillatoria (OSC)	black puffs	*Oscillatoria*	Carmabi station; Curacao	12°07'23.2"N	68°58'09.4"W	>2m	Viridamides A-B. malyngamide C acatata(MN)
PAC22JUN14-2 (PAC)	L=2.5 um, W=5 um, red puffs	*Spirulina*	Coiba, Panama	N/A	N/A		N/A
ASG15JUL14-6 (ASG)	red puffs	*Spirulina major*	American Samoa	N/A	N/A		N/A
PAL24MAY13-5, cont A (PAL-contA)	pink unicells; purple suspension 10-15um	N/A	Dolphins (Airstrip W end), Palmyra Atoll	5.884889°N	162.084519°W	1 m	N/A

3.3.2 Media preparation

SWBG11 media is prepared with standard Gerwick lab protocol (Moss *et al.*, 2018).

3.3.3 Cryopreservation of cyanobacteria

Standard Protocol

The standard protocol for cryopreservation of our marine cyanobacteria was adapted from the UTEX Culture Collection of Algae at the University of Texas at Austin with minor changes. Samples (0.9 mL in SWBG11 medium) were mixed with 0.9 mL sterile cryo-protective additive media (2x concentration) into a 2 mL cryovial to give a final concentration of 5% or 10% (v/v) dimethylsulfoxide (DMSO). For cyanobacteria from the genus *Moorena* and *Leptolyngbya*, the sheets or filaments were cut to approximately 1-inch in length before being placed into individual vials with aseptic technique. The vials were incubated for at least 5 minutes before being placed in a pre-chilled (minimum 24 hours) Nalgene Mr. Frosty container containing isopropanol. The freezing container was placed in a -80 °C freezer for 2 hours. The vials were then transferred to a rack and placed into liquid nitrogen dewar for long-term storage.

After 1 week of storage in liquid nitrogen, the vials were removed and placed into a ~37 °C water bath for ~2 min with slight agitation to remove ice crystals. The vials were centrifuged for 5 minutes at 2000 RPM to pellet the cyanobacteria. The cryo-media was decanted and replenished with fresh SWBG11 media. After incubation for 10 minutes, the vials were once again subjected to centrifugation for 5 minutes at 2000 RPM before the media was decanted. Each culture was placed into a well in a 12-well plate with 3 mL of fresh media. The plates were immediately placed in the culture room in complete darkness for 24 hours at 27 °C. After 24 hours, the plates were returned to normal lighting conditions and monitored weekly for growth.

3.3.4 Alterations to Standard Protocol

Methanol as CPA

Methanol was used as a CPA at a concentration of 5 and 10% (v/v). Standard cryopreservation was followed as listed above.

Reduced growth media and salinity

SWBG11 medium was prepared with half the amount of Instant Ocean (16.5 g/L) to reduce the salinity in the cryo-media. Reduced salinity. SWBG11 media was used for CPA mixture preparation and microbial suspension in cryo-vials. The remaining cryopreservation standard protocol was followed as listed above. Similarly, half-strength SWBG11 medium was prepared by reducing concentration of BG stocks 1-9 by half in the cryo-media. This half-strength SWBG11 was used for CPA mixture preparation and microbial suspension in cryo-vials. The remaining standard protocol was followed as listed above.

Addition of Proline as non-penetrating CPA

Proline was added to the cryo media to alter osmolality during post-thaw conditions. There has been some record of the ability of proline to increase recovery potential of cryopreserved cultures when compared to DMSO and glycerol (Withers and King, 1979). Proline was added to SWBG11 media to reach a final concentration of 20 and 200 mM in the cryo media. Standard freezing and thawing protocol were followed thereafter.

Nitrogen enriched post-thaw media

SWBG11 media was prepared with 2 times and 3 times that amount of nitrogen by doubling and tripling the amount of BG#1 [$NaNO_3$] added. Samples were cryopreserved with standard protocol. For post-thaw growth recovery, nitrogen-enriched media was used in place of regular SWBG11.

3.3.5 Post-thaw viability assessment and monitoring

Cultures were monitored on a weekly basis for any changes in growth recovery. A colorimetric scale was developed for each culture based on bleaching of the culture or return to normal condition. Similarly, all cultures were inspected by microscopy every 30 days for cell shrinkage or normal morphology. If enough active growth was present in the culture, LCMS analysis of the metabolic profile was compared to culture grown at normal conditions. Similarly, morphological analysis was conducted by inspection by microscope every 30 days.

3.4 Results

3.4.1 *Leptolyngbya* sp.

ISBNOV94-8A

The best growth recovery was observed in all samples of ISB-8A. Previous attempts to cryo-preserve this culture were successful as well. Therefore, in this study, we sought to observe the effects of long-term preservation of this culture. Cultures that were preserved for 1 week, 2 weeks, 6 weeks, 3 months, 6 months, and 1 year all responded well to cryopreservation with 15% DMSO and storage in a liquid nitrogen dewar (**Figure 2.1**). In normal culturing conditions, ISB8A cultures consist of thin, deep purple filaments that arrange into a mat. After taking the cryo-samples out of the freezer, all samples were pale-yellow and bleached in color. Purple flecks began to show after 30 days post-thaw indicating the start of return to normal culturing conditions. The only variation to this pattern was observed in the samples that were preserved for 3 months. Two out of the three replicates took longer than 30 days before purple flecks began to return to the cultures. After 60 days post-thaw, all samples fully regained their purple hue and began rapid growth.

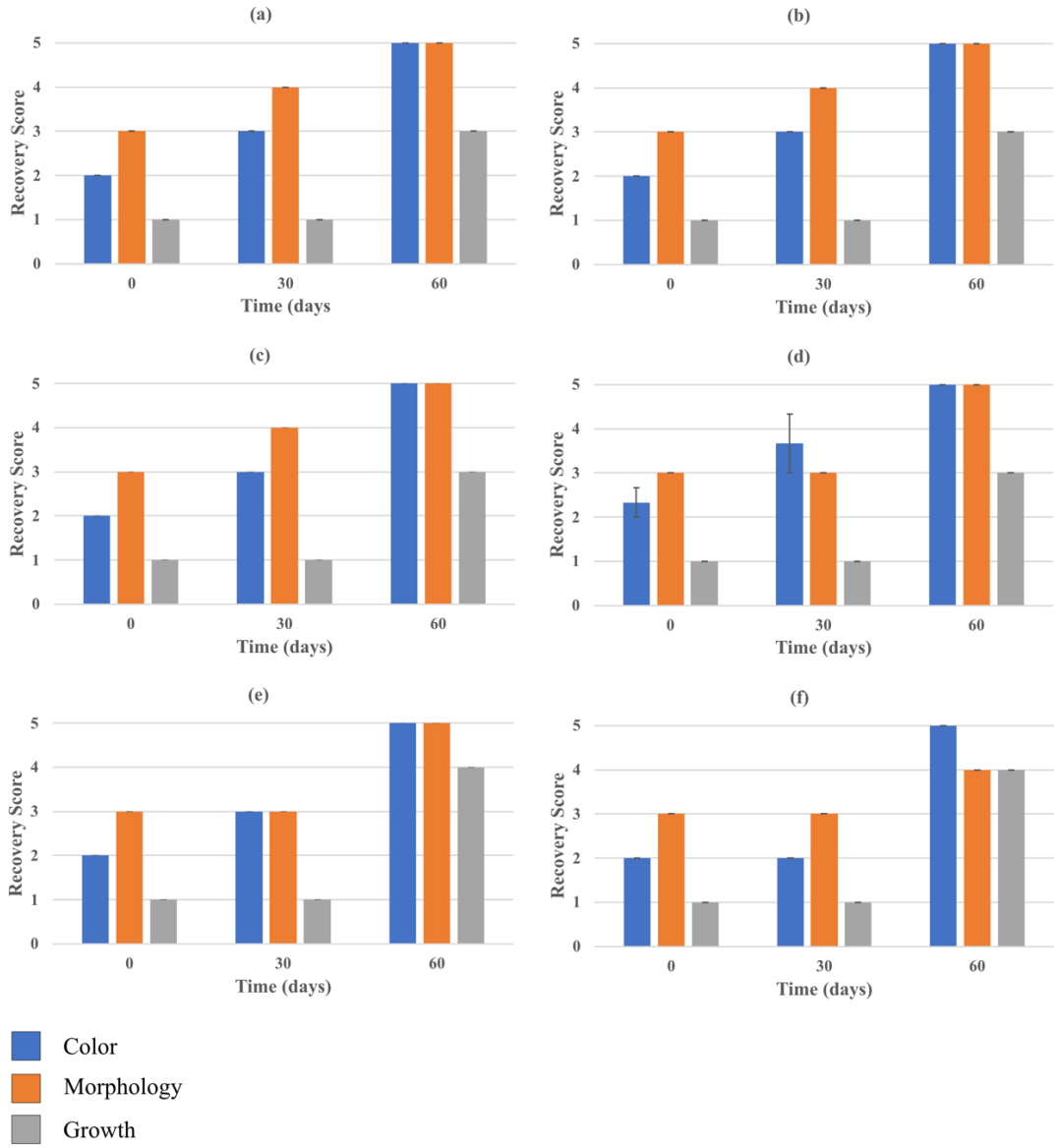

Figure 3.1 Growth recovery for ISB3NOV94-8A after cryopreservation for (a) 1 week, (b), 2 weeks, (c) 6 weeks, (d) 3 months, (e) 6 months, and (f) 1 year.
Samples were prepared in triplicate for each duration of cryopreservation. Timepoints are recorded in days post-thaw. All samples were cryopreserved with 15% DMSO and standard protocol. Color of the samples (bleached-white to deep purple) was graded from 1-5. Morphology of the samples (shrunken cells to full-size) was graded from 1-5. Growth (no growth to active growth) was graded from 1-5. Standard error bars are for each mean are presented.

Metabolomic analysis of these cultures by LCMS revealed a novel distinct peak of 958 *m/z*. All cultures were subjected to crude extraction on or after 140-days post-thaw. The novel distinct peak of 958 *m/z* is present in all samples cryopreserved at the different time-points

(Figure 3.2a). Interestingly, there was a relatively low production of a previously described major secondary metabolite, leptochelin (897 *m/z*). Molecular networking of the different conditions revealed a novel cluster of nodes associated with the new distinct peak at *m/z* 958.

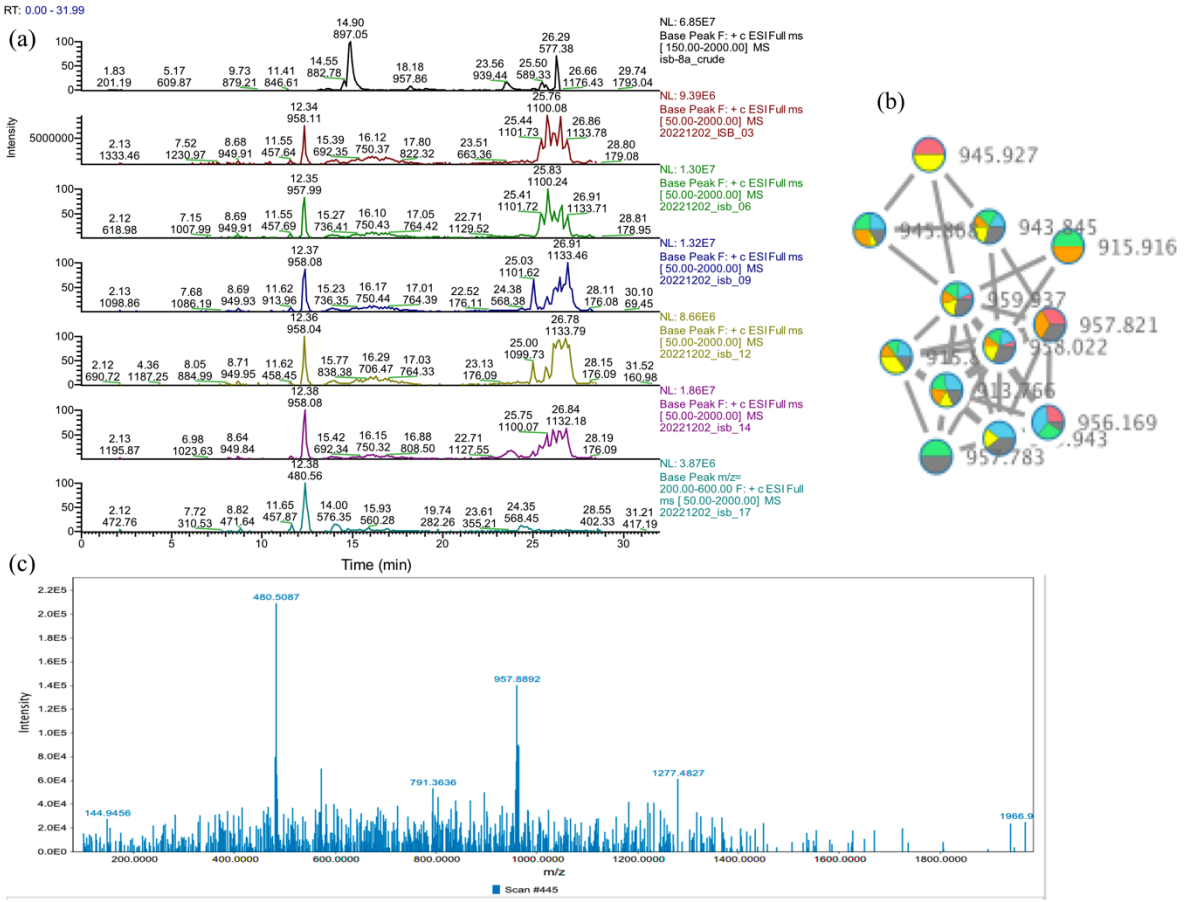

Figure 3.2 Metabolomic analysis by LCMS of long-term cryopreserved ISB8A reveals novel compound. (a) Chromatograms of crude extract from normal ISB8A (black), 1-week cryo (red), 2-week cryo (green), 6 week cryo (blue), 3 month cryo (yellow), 6 month cryo (magenta), and 1 year cryo (teal). (b) Cluster of nodes within the crude extract of ISB8A. Red: normal ISB8A, Blue: 1-week cryo, Green: 2-week cryo, orange: 6 week cryo, yellow: 3 month, gray: 6 month and 1 year cryo. (c) MS1 fragmentation of novel distinct peak of 958 m/z.

Leptolyngbya sp. ASX22JUL14-2a

For *Leptolyngbya sp.* ASX, growth recovery was observed in both 5% and 10% DMSO treatments with storage in liquid nitrogen for 1 week (Figure 3.3a, b). During normal culture conditions, ASX consists of thin, green filaments arranged into a dense mat with dark green flecks randomly dispersed throughout. All the replicates in 5% and 10% DMSO retained green

sheet color immediately post-thaw. After 30 days post-thaw, the filaments turned to a pale-yellow hue with dark green speckled throughout the sheet. Additionally, biofilms began to form along the sides of the wells. By 60 days post-thaw, all replicates were mostly dark green with some flecks of green clumps with visible active growth.

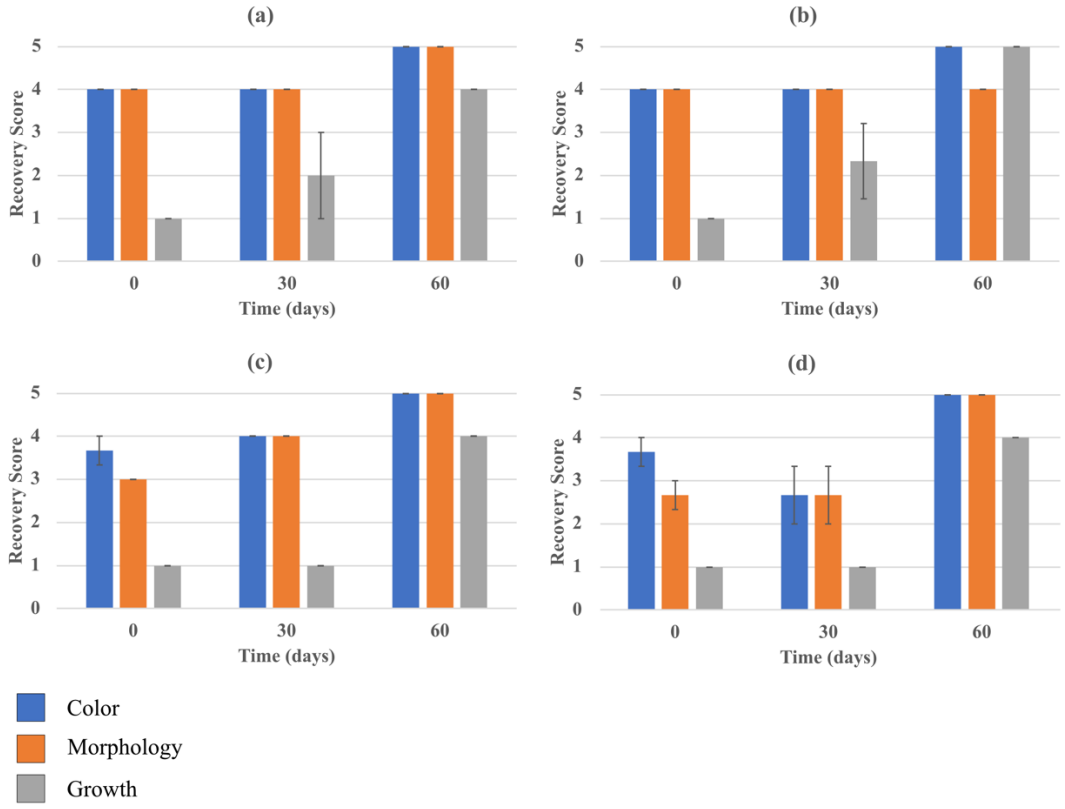

Figure 3.3 Growth recovery for ASX22JUL14-2a at 5 (a) and 10 % (b) DMSO and 3L-Oscillatoria at 5 (c) and 10 % (d) DMSO.
Samples were prepared in triplicate for each CPA concentration. Timepoints were recorded in days post-thaw. Samples were cryopreserved with standard protocol. Color of the samples (bleached-white to green/black) was graded from 1-5. Morphology of the samples (shrunken cells to full-size) was graded from 1-5. Growth (no growth to active growth) was graded from 1-5. Standard error bars for each mean are presented.

3.4.2 3L-*Oscillatoria*

For 3L-*Oscillatoria* (OSC), the maximum recovery was recorded in 5% DMSO rather than 10% DMSO after 7 days of cryopreservation (Figure 3.3c, d). Two out of the three replicates in 10% DMSO died after 30 days. After 60 days, the visual growth was observed in the remaining cultures. In the regularly maintained cultures, OSC contains thin, brown filaments

with green clumps of cells. However, in all the surviving cryo-cultures, the green clumps were largely absent.

3.4.3 *Moorena* sp.

Moorena bouillonii GFR15JUN17-1

For *M. bouillonii* GFR (GFR), moderate growth recovery was observed in cultures treated with 5% and 10% DMSO and storage in liquid nitrogen for 1 week. In normal culturing conditions, GFR consists of thin, hair-like brown filaments. Immediately post-thaw, the filaments in GFR were pale green and almost naked to the eye. After 30 days post-thaw, 2 out of the 3 replicates in each treatment were bleached white in color and completely dead. The remaining cultures had no noticeable difference to treatment with 5% or 10% DMSO. The filaments were brown and looked morphologically like normal cultures for GFR. After 60 days post-thaw, the cultures looked healthy but there was no active growth observed. Unfortunately, after 90 days post-thaw, the remaining cultures became bleached-white and there was no active growth.

Moorena ASY22JUL14-1

For *Moorena sp.* ASY (ASY), all replicates in 5% and 10% DMSO treatment were not able to be successfully cryopreserved. Immediately post-thaw, the dark green filaments turned into light green and yellow hair-like filaments. After 30 days post-thaw, all cultures had pale yellow and bleached filaments. By microscopic evaluation, the sheaths containing the cyanobacteria were completely absent of any healthy cells.

Moorena bouillonii PNG5-198

For *M. bouillonii* PNG (PNG), poor recovery was observed in samples treated in 5% and 10% DMSO after 7 days of cryopreservation in liquid nitrogen. Replicates treated with 10%

DMSO had more pigmented filaments and large cells after being taken out of cryo-storage. After 30 days post-thaw, the filaments in all the replicates were pale yellow and bleached. The sheaths of the filaments were nearly empty of cells or had cells that were shrunken in size.

Moorena producens PAL15AUG08-1

For *M. producens* PAL (PAL), poor recovery was observed in sample treated in 5% and 10% DMSO after 7 days of cryopreservation in liquid nitrogen. Markedly, all samples became bleached and lost all pigments within 48 hours post-thaw. The sheaths of the filaments were completely absent of cells or had cells that were reduced in size.

Moorena producens JHB22AUG96-1

In a similar fashion to other *Moorena* sp., *M. producens* JHB (JHB) had the poorest recovery out of all *Moorena* sp. under the standard treatment. Within 7 days of post-thaw, the filaments all looked bleached and were devoid of cells in the sheaths. Therefore, JHB was selected for further optimization studies with the rationale that if we could successfully cryopreserve our largest *Moorena sp.*, we could apply the same strategies to the other *Moorena* strains that were unable to be cryopreserved with the standard method.

The first alternative treatments applied to JHB involved the use of alternative cryoprotective agents. Methanol (MeOH) was selected as an alternative penetrating CPA (pCPAs) and sucrose and proline were selected as alternative non-penetrating CPAs (npCPAs). Unfortunately, each of the CPAs applied were not able to successfully preserve JHB for longer than 1 week. The use of MeOH exhibited the worst post-thaw viability. Immediately post-thaw, the samples turned to a red brown color. After 24 hours, all samples were completely bleached and devoid of color. For sucrose and proline treatment, cell morphology was mostly normal immediately post-thaw. However, after 2 weeks post-thaw, cells began to shrink in size and all

samples turned to a yellow color. After 1-month post-thaw, all cells showed no improvement in their growth recovery and remained a pale-yellow color. Overall, modulation of the CPA did not improve on the growth recovery of JHB after cryopreservation. Perhaps exploring a different concentration or combination of multiple CPAs could work to improve post-thaw viability of this culture.

The next alternative treatment applied to JHB involved modulation of the thawing rate to prevent the formation of intracellular ice crystals during the thawing process. Samples were either subjected to the standard protocol of rapidly thawing or thawing at room temperature for 2 hours. There was no observable difference between samples that were rapidly thawed or slow thawed. Immediately post-thaw, all the samples were light green in color and some cells were shrunken in the sheaths. After 48 hours post-thaw, the cells were severely shrunken in size and the cultures became a pale-yellow color. At 30 days post-thaw, all samples in both conditions were bleached white and did not show any noticeable growth.

The last alternative treatment applied to JHB involved altering the concentration of solutes in the media for cryopreservation and for post-thaw growth recovery. Reducing the overall extracellular solute concentration could reduce the efflux of water out of the cells immediately post-thaw. This could help the cells retain their normal size and improve growth recovery. However, there was no noticeable difference between reducing the concentration of solutes in the growth media compared to the standard protocol. Like the results described above, JHB became bleached within 24 hours of post-thaw. Subsequently, the next modulation to the standard protocol that was applied was to enrich the post-thaw media with nitrogen. Cyanobacteria can enter a chlorotic state of dormancy to survive extended periods of nitrogen starvation. When nutrients are reintroduced to the cyanobacteria, their light-harvesting

complexes, phycobilisomes, will return and the cells will return to regular vegetative growth (Spät et al., 2018). Samples were cryopreserved with the standard protocol and 10% DMSO. However, instead of using regular SWBG11 media post-thaw, SWBG11 with 2x and 3x nitrogen-enriched media was used. There was no noticeable difference or change in the growth recovery of the any of the samples for either of the conditions. Cell shrinkage occurred within 24 hours post-thaw.

3.4.4 Spirulina sp.

Spirulina major ASG15JUL14-6

For ASG15JUL14-6 (ASG), poor recovery was also observed in all samples in both treatments with the standard protocol (**Figure 3.2ab**). In normal culturing conditions, ASG's red and pink spiral filaments arrange into sheets. Immediately post-thaw, the sheets of ASG turned to a light green color with light pink edges. After 30 days post-thaw, the sheets remained light green in color but there was no active growth. There was no noticeable difference between samples prepared with 5% or 10% DMSO. After 60-days post-thaw, there was no improvement to the color, morphology or growth compared to 30 days prior.

Spirulina sp. PAC22JUN14-2

For PAC22JUN14-2 (PAC), poor recovery was observed in all samples in both treatments with the standard protocol (**Figure 3.2.b, c)** During regular culturing conditions, PAC has red and pink filaments that arrange themselves into a sheet. Immediately post-thaw, the sheets turned to a lime-green color. After 30 days, 1 out of the 3 replicates in each condition became completely bleached white and were not chosen to continue with growth recovery. The remaining samples were pale yellow in color likely due to the cells shrinking in size. After 60

days post-thaw, one replicate in 10% DMSO retained the pale-yellow color observed above. However, the remaining samples became bleached white.

3.4.5 PAL24MAY13 – contA

PAL-contA demonstrated a good recovery in 5% and 10% DMSO treatment after 30 days post-thaw. There was no noticeable difference between the 5% and 10% DMSO treatments. The unicells were bright pink and purple and aggregated into clumps. However, after 60 days post-thaw, 4 out of the 6 cultures died and could not be recovered. One of the remaining cultures in 10% DMSO died several days later followed by the 5% DMSO treatment.

3.5 Discussion

In this screening study to develop an optimal method for cryopreservation of tropical marine cyanobacteria, only a few cultures were able to be cryopreserved successfully. Both species of the genus *Leptolyngbya* were able to be successfully cryopreserved with great growth recovery. The filaments of *Leptolyngbya* sp. arrange into microbial mats which consists of exopolysaccharides (EPS). EPS have previously been shown to be a viable CPA for the cryopreservation of bacteria and cyanobacteria. They have the added benefit of being loss toxic compared to other used CPAs like DMSO and MeOH. For example, Ali and others (2021) extracted EPS from a glacier bacterium and used it to cryopreserve cyanobacteria and microalgae. They found that cultures cryopreserved with EPS showed better growth recovery compared to cultures preserved commonly used CPAs like DMSO or glycerol (Ali et al., 2021). The EPS in the mats of both *Leptolyngbya* species could play a role in the growth recovery of the cultures. As mentioned previously, one of the factors that can affect growth recovery is the solute concentration during freezing and post-thaw. The stability of the EPS in the sheets could work to

maintain the solute concentration in the cells and facilitate efficient efflux of intracellular water during freezing. In a similar fashion, the EPS in the sheets could also prevent the rapid influx of water into the cells after cryopreservation. This could prevent rupturing of the cells and facilitate optimal growth recovery. Further exploration into the use of EPS as CPA to preserve these cyanobacteria more efficiently could be fruitful.

The most intriguing result was that the metabolomic profile of ISB was altered after cryopreservation. A novel distinct peak of 958 *m/z* was observed in all samples regardless of the duration of cryopreservation. This 958 *m/z* peak was also observed in normal cultures ISB. This compound could play a role in the growth recovery of ISB considering that it was produced in higher quantities relative to the regularly maintained culture of ISB. This compound could be produced in response to a highly stress-induced, cold environment. Further explorations into the identity of this compound through isolation and structure elucidation can gave us some insight on its role in the cryopreservation of this species. Additionally, the method employed with ISB may need to be amended if the goal of cryopreservation is to preserve the genomic stability as well as metabolomic profile of this species. It will also be interesting to evaluate if this is a permanent alteration in the metabolome of this strain, or if over time it returns to a metabolome similar to the starting culture.

The cultures of the *Moorena* genus were not able to be cryopreserved with any of the standard protocols. Interestingly, immediately post-thaw, the cryo-media that the cultures resided in all became pigmented in pink and purple colors before the first media change. Cyanobacteria can enter a dormant, chlorotic state during periods of nitrogen starvation. During the stage of chlorosis, their light harvesting complexes, phycobilisomes, become rapidly degraded (Spät et al., 2018). The *Moorena* species cyanobacteria used in this study likely entered a chlorotic state

during cryopreservation. This resulted in the excretion of the degraded phycobilisomes proteins. More specifically, the pigments were likely phycoerythrin or phycocyanin. The degradation of their light-harvesting complexes most likely made it difficult for these cultures to recover from cryopreservation. Although they were returned to regular growth conditions, the cultures were likely unable to reconstitute their light-harvesting complexes which would facilitate photosynthesis, and subsequently, growth recovery.

In conclusion, further optimization studies will need to be conducted in order to successfully cryopreserve many of the cyanobacterial cultures in the Gerwick lab collection. Further testing with different CPAs than the ones used in this study could facilitate better growth recovery.

3.6 References

Ali, P., Fucich, D., Shah, A. A., Hasan, F., & Chen, F. (2021). Cryopreservation of Cyanobacteria and Eukaryotic Microalgae Using Exopolysaccharide Extracted from a Glacier Bacterium. *Microorganisms*, *9*(2), 395. https://doi.org/10.3390/microorganisms9020395

Day, J. G. (2007). Cryopreservation of Microalgae and Cyanobacteria. In J. G. Day & G. N. Stacey (Eds.), *Cryopreservation and Freeze-Drying Protocols* (pp. 141–151). Humana Press. https://doi.org/10.1007/978-1-59745-362-2_10

Jang, T. H., Park, S. C., Yang, J. H., Kim, J. Y., Seok, J. H., Park, U. S., Choi, C. W., Lee, S. R., & Han, J. (2017). Cryopreservation and its clinical applications. *Integrative Medicine Research*, *6*(1), 12–18. https://doi.org/10.1016/j.imr.2016.12.001

Moss, N. A., Leao, T., Glukhov, E., Gerwick, L., & Gerwick, W. H. (2018). Chapter One—Collection, Culturing, and Genome Analyses of Tropical Marine Filamentous Benthic Cyanobacteria. In B. S. Moore (Ed.), *Methods in Enzymology* (Vol. 604, pp. 3–43). Academic Press. https://doi.org/10.1016/bs.mie.2018.02.014

Pegg, D. E. (2007). Principles of Cryopreservation. In J. G. Day & G. N. Stacey (Eds.), *Cryopreservation and Freeze-Drying Protocols* (pp. 39–57). Humana Press. https://doi.org/10.1007/978-1-59745-362-2_3

Spät, P., Klotz, A., Rexroth, S., Maček, B., & Forchhammer, K. (2018). Chlorosis as a Developmental Program in Cyanobacteria: The Proteomic Fundament for Survival and Awakening. *Molecular & Cellular Proteomics : MCP*, *17*(9), 1650–1669. https://doi.org/10.1074/mcp.RA118.000699

Withers, L. A., & King, P. J. (1979). Proline: A Novel Cryoprotectant for the Freeze Preservation of Cultured Cells of Zea mays L. *Plant Physiology*, *64*(5), 675–678.

3.7 Acknowledgements

Chapter 3, in part, has been facilitated by the work of Syrena Whitner, Nathan Moss, Andrew Ecker, Sebastian Rohrer, and Yifan He. Their previous work on developing a cryopreservation method for the cyanobacteria have paved the way for these optimization studies. I'd also like to acknowledge Dr. Evgenia Glukhov for providing the cultures used in this work and for feedback on growth recovery and health of the cultures.

Conclusion

4.1 Insights into the Metabolic potential of *Moorena producens* JHB

In Chapter 2, the co-culture competition experiment with JHB and *C. albicans* led to the discovery of a novel depsipeptide, hectoramide B. The fragmentation pattern and NMR spectra of this novel compound bore resemblance to previously described hectoramide A (Boudreau et al., 2015). This finding led to the elucidation of the structure of hectoramide B. Hectoramide A is likely a degradation product of hectoramide B because it only contains the final 3 residues found in hectoramide B.

Genomic analysis of the draft genome of JHB revealed some potential candidate biosynthetic gene clusters associated with hectoramide B production. Regeneration of sequencing data allowed for the reassembly of the JHB genome and improved quality compared to the previous iteration. Subsequently, this led to discovery of the putative biosynthetic gene cluster responsible for the production of hectoramide B.

Using bioinformatic analyses, we were able to putatively identify the hectoramide B (hca) pathway. Sequence alignments, phylogenetic trees, and structural alignments allowed us to elucidate the initial annotated regions in the gene cluster. This revealed some interesting enzymatic activity within the gene cluster like the incorporation of an α-hydroxy acid residue, and the absence of a termination mechanism.

To further characterize and confirm the identity of the biosynthetic gene cluster of hectoramide B, additional efforts are needed to express the different enzymatic domains in the gene cluster. More specifically, analysis into the hcaB adenylation domain's preferred ligand could reveal some interesting enzymology.

Although hectoramide B did not exhibit antifungal activity against *S. cerevisiae*, further studies are needed to determine the ecological reason for the upregulation of this compound. Since other known metabolites produced by JHB were also found to be upregulated, like jamaicamide A and C, hectoramide B could have a synergistic role with these other metabolites.

Overall, this work reveals that the metabolic and biosynthetic potential of JHB could still be explored for novel natural products. Most depsipeptides are cyclic so there is limited precedence of a linear depsipeptide. Furthermore, the selection of an α-hydroxy acid version of tyrosine is even more intriguing. Evidently, JHB contains some interesting enzymology that should be further explored. Additionally, co-culture experiments can be an efficient method for the discovery of novel natural products. This method could be applied to other strains in the Gerwick cyanobacterial collection in order to discover new bioactive natural products.

4.2 Insights into the Cryopreservation of cyanobacteria

In Chapter 3, we were able to show that some strains in the Gerwick lab collection were able to be successfully cryopreserved. These strains are a valuable source of therapeutically relevant molecules, and a method needs to be developed to maintain the metabolic and genomic stability of these organisms. Unfortunately, most of the strains used in this work were unable to be cryopreserved. However, the results observed will pave the way for different and new strategies to find an optimal and viable cryopreservation method.

We also were able to identify a novel secondary metabolite through the cryopreservation of *Leptolyngbya* strain ISB. Although the metabolomic profile was altered with this cryopreservation method, it may also open new possibilities to discover novel secondary metabolites. The discovery of new natural products via subjecting microbes to stress-induced environments is not a novel idea. However, there is limited precedence on applying a freeze or

cold-stressor on a microbe to see what kind of new secondary metabolites may be produced. Further exploration into the role of this novel compound may give some insight on new cryopreservation methods or new avenues for natural product discovery.

Appendix

5.1 Chapter 2

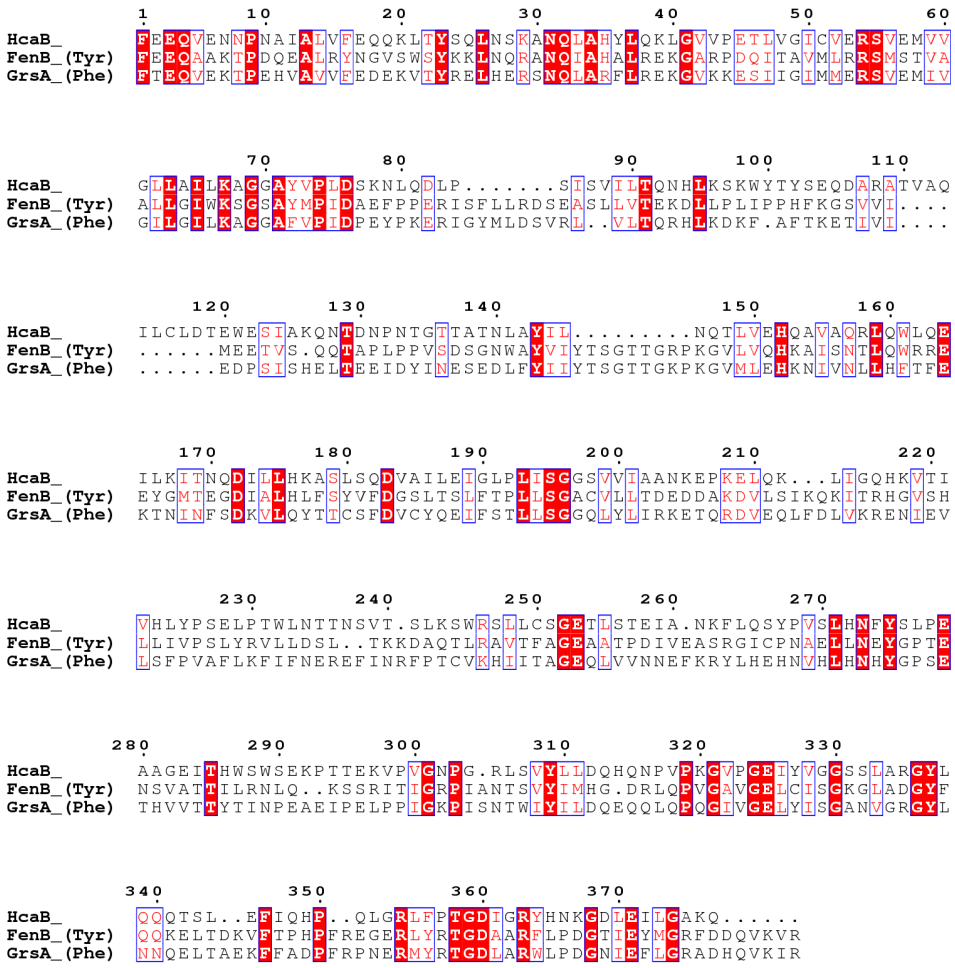

Figure A.1 Full Sequence alignment of hcaB adenylation domain with other NRPS adenylation domains.

5.2 Chapter 3

Table A.1 Recovery scores of cyanobacteria cryopreserved in this study.
All cultures were cryopreserved with either 5 or 10% DMSO (v/v) as cryoprotective agent except for ISBNOV94-8A (cryopreserved with 15% DMSO). All cultures were subjected to standard protocol. Growth scores range from 1-5 based on color, morphology, and growth. The scores were recorded at Day 0, Day 30, and Day 60 post-thaw. JHB and PAL were excluded from this chart because they were not able to survive past day 7.

Culture Name	Day 0			Day 30			Day 60			Day 0			Day 30			Day 60		
	3	3	1	2	1	1	1	1	1	4	3	1	2	1	1	1	1	1
	3	3	1	0	0	0	0	0	0	4	2	1	0	0	0	0	0	0
ASG14JUL14-6	3	3	1	3	2	1	3	2	1	4	3	1	3	2	1	2	2	1
	4	3	1	4	4	1	5	5	4	3	3	1	4	4	1	5	5	4
	3	3	1	4	4	1	5	5	4	4	3	1	2	2	1	0	0	0
3L-Oscillatoria	4	3	1	4	4	1	5	5	4	4	2	1	2	2	1	0	0	0
	3	3	1	2	2	1	1	2	1	3	3	1	3	3	1	3	3	1
	3	3	1	2	2	1	2	2	1	3	3	1	2	2	1	2	2	1
PAC22JUL14-2	3	3	1	2	2	1	0	0	0	3	3	1	3	3	1	0	0	0
	4	4	1	4	4	1	0	0	0	4	4	1	4	3	1	0	0	0
	4	4	1	2	2	1	0	0	0	4	3	1	2	2	1	0	0	0
PAL24MAY13 - contA	4	4	1	2	2	1	0	0	0	4	3	1	3	2	1	0	0	0
	2	3	1	1	1	1	0	0	0	2	3	1	1	1	1	0	0	0
	2	3	1	1	1	1	0	0	0	3	3	1	2	1	1	0	0	0
PNG5-198	2	3	1	1	1	1	0	0	0	3	3	1	1	1	1	0	0	0
	3	2	1	1	1	1	0	0	0	3	2	1	1	1	1	0	0	0
	3	2	1	4	4	1	5	4	1	3	2	1	4	4	1	5	4	1
GFR15JUN17-1	3	2	1	1	1	1	0	0	0	3	2	1	1	1	1	0	0	0
	3	4	1	1	2	1	0	0	0	3	4	1	1	2	1	0	0	0
	3	4	1	1	2	1	0	0	0	3	4	1	1	2	1	0	0	0
PAB18MAY11-9	3	4	1	1	2	1	0	0	0	3	4	1	1	2	1	0	0	0
	4	4	1	4	4	1	5	5	4	4	4	1	4	4	1	5	4	5
	4	4	1	4	4	4	5	5	4	4	4	1	4	4	4	5	4	5
ASX22JUL-14-2	4	4	1	4	4	1	5	5	4	4	4	1	4	4	2	5	4	5
	2	2	1	1	1	1	0	0	0	2	2	1	2	2	1	0	0	0
	3	3	1	2	1	1	0	0	0	2	2	1	1	1	1	0	0	0
ASY22JUL14-1	3	3	1	1	1	1	0	0	0	3	3	1	1	1	1	0	0	0
	2	3	1	3	4	1	5	5	3	2	3	1	3	4	1	5	5	3
	2	3	1	3	4	1	5	5	3	2	3	1	3	4	1	5	5	3
ISBNOV94-8A (a)	2	3	1	3	4	1	5	5	3	2	3	1	3	4	1	5	5	3
	2	3	1	3	4	1	5	5	3	3	3	1	5	3	1	5	5	3
	2	3	1	3	4	1	5	5	3	2	3	1	3	3	1	5	5	3
ISBNOV94-8A (c)	2	3	1	3	4	1	5	5	3	2	3	1	3	3	1	5	5	3
	2	3	1	3	3	1	5	5	4	2	3	1	2	3	1	5	4	4
	2	3	1	3	3	1	5	5	4	2	3	1	2	3	1	5	4	4
ISBNOV94-8A (e)	2	3	1	3	3	1	5	5	4	2	3	1	2	3	1	5	4	4
				5% DMSO									10% DMSO					

Growth score

Color
Morphology
Growth

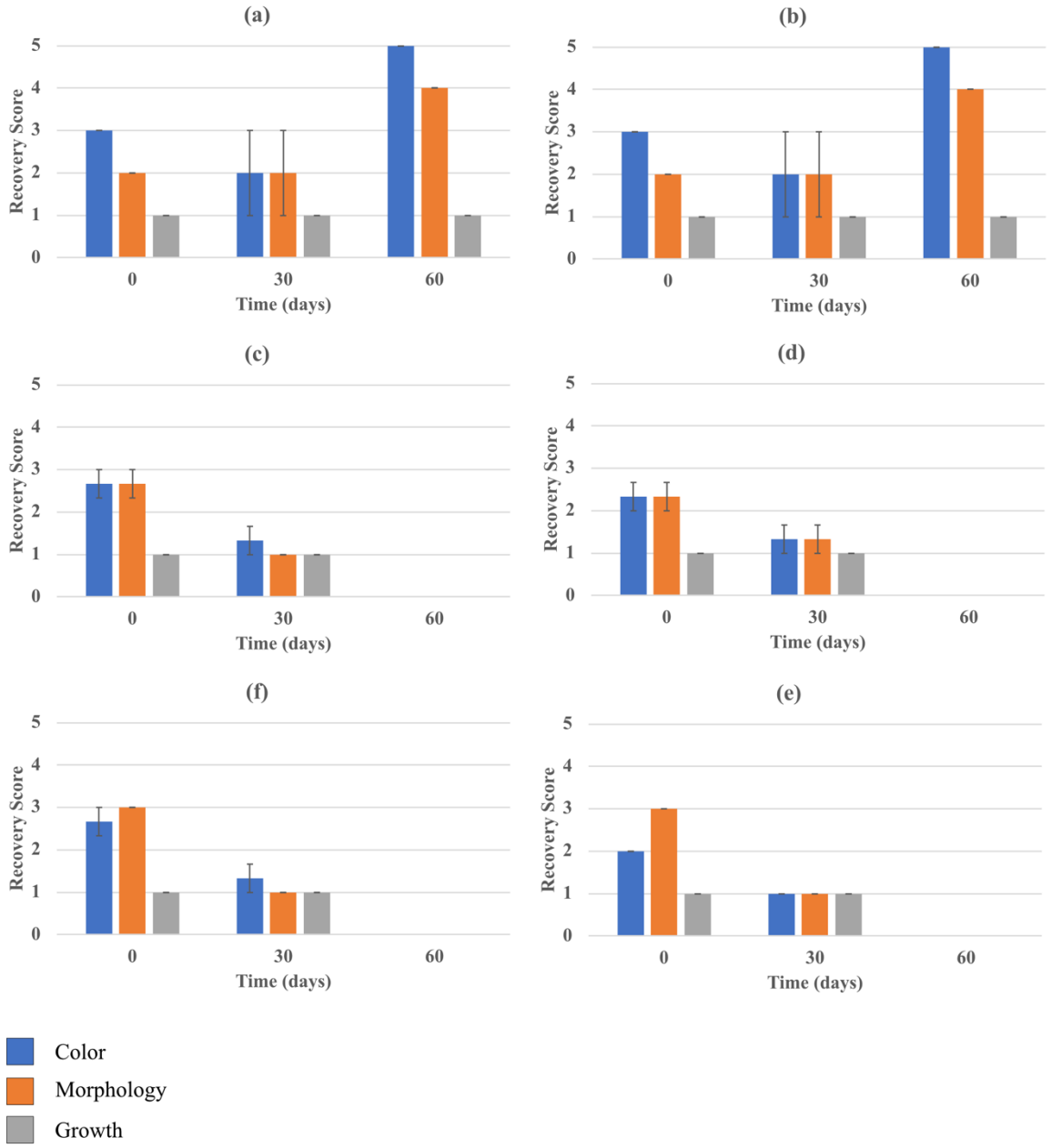

Figure A.2 Growth recovery for GFR at 5 (a) and 10 % (b) DMSO, ASY at 5 (c) and 10 % (d) DMSO, and PNG at 5 (e) and 10 % (f) DMSO.
Samples were prepared in triplicate for each CPA concentration. Timepoints were recorded in days post-thaw. Samples were cryopreserved with standard protocol. Color of the samples (bleached-white to green/brown) was graded from 1-5. Morphology of the samples (shrunken cells to full-size) was graded from 1-5. Growth (no growth to active growth) was graded from 1-5. Standard error bars for each mean are presented.

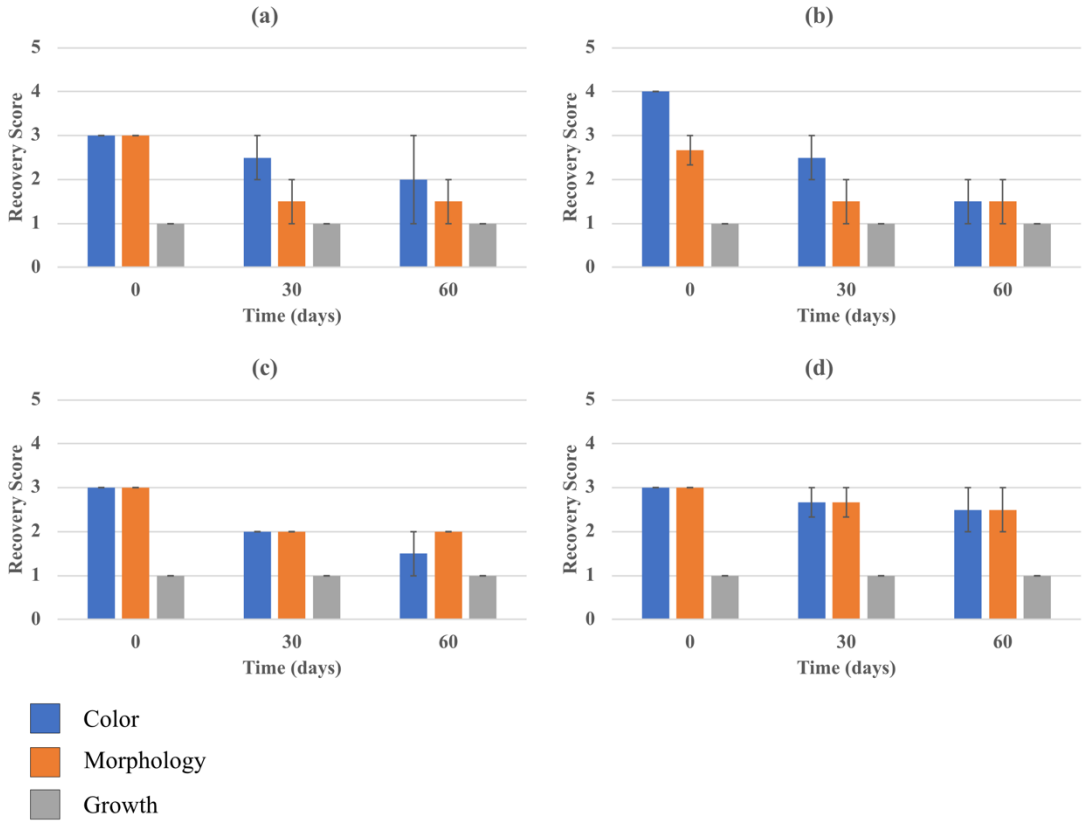

Figure A.3 Growth recovery for ASG at 5 (a) and 10% (b) DMSO and PAC at 5 (c) and 10 % (d) DMSO. Samples were prepared in triplicate for each CPA concentration. Timepoints were recorded in days post-thaw. Samples were cryopreserved with standard protocol. Color of the samples (bleached-white to pink/red) was graded from 1-5. Morphology of the samples (shrunken cells to full-size) was graded from 1-5. Growth (no growth to active growth) was graded from 1-5. Standard error bars for each mean are presented.